

We thank the reviewer for the insightful and constructive comments. We have made point-by-point responses and/or revisions according to your suggestions and instructions. We recall the comments of the reviewer in black, followed by our reply in blue.

Please note that we have rerun the simulations involving RUN(3) as replied to the comment #3 from referee #2, and all the figures in the manuscript have been revised accordingly.

The revised manuscript with tracking of all the changes that have been made is appended at the end of this response.

### **Responses to Referee #1**

#### **Anonymous Referee #1**

Received and published: 15 September 2020

The authors systematically evaluated the effects of different physical processes and associated parameterization options on Noah-MP simulated soil temperature at a permafrost site over the Tibetan Plateau. The manuscript is generally well-written and well-structured. Before it can be considered for potential publication, I have a few comments for the authors to consider.

Major comment:

1. I am not convinced why the authors did not test the snow-related processes and parameterizations, such as snow albedo and rain-snow partitioning schemes. These processes along with the snow cover formulation in Noah-MP will affect surface heat fluxes and energy balance, which can potentially affect soil temperature evolution below snowpack. Particularly, the authors found that Noah-MP generally underestimates the soil temperature during the cold season, which could partially be related to snowpack simulations. The authors also did not tell the readers that what parameterization schemes they used for snow albedo and partitioning processes.

Moreover, a recent study over Tibetan Plateau (Jiang et al., 2020,

<https://agupubs.onlinelibrary.wiley.com/doi/abs/10.1029/2020JD032674>) showed that the processes already tested by the authors here along with the snow cover formulation can significantly affect snowpack simulations, which could further affect soil conditions. Thus, it is likely that the processes the authors tested can indirectly affect soil conditions through modifying snowpack. I suggest the authors add some discussions on this aspect and include some quick tests for snow-related processes if possible.

**Response:** Thank you for your constructive suggestion! In the revised manuscript, we have conducted an ensemble of 41472 (= 6912\*2\*3) experiments to test the performance of Noah-MP in simulating snow processes. Results show that Noah-MP extremely overestimates the albedo and thus induces great cold bias in soil temperature. Detailed results and discussions are illustrated in the newly added Sec. 3.1.1 and Sec. 4.1, respectively.

In addition, snow process is not considered by setting the snow fraction in precipitation to zero in this study. Since no snow cover in the ground, the ground albedo equals the soil albedo. We have added some explanations in lines 164-167: "For practical purpose, the ALB and SNF processes were not considered by setting the snow fraction in precipitation to zero. Since no snow cover in the ground, the ground albedo equals the soil albedo".

Minor comments:

1. Line 108: "depth" -> "depths".

**Response:** Revised as suggested.

2. Line 170: Please give some details on how the soil column was discretized, e.g., how many soil layers, the thickness of each layer, etc.

**Response:** The details of each layer are listed in the supplementary file as Table S1:

**Table S1** Soil discretization scheme and soil particle fraction in this study.

Layer	$Z_i$	$\Delta Z_i$	$Z_{h,i}$	Sand (%)	Silt (%)	Clay (%)
-------	-------	--------------	-----------	----------	----------	----------

1	0.010	0.020	0.020	85.48	12.59	1.93
2	0.040	0.040	0.060			
3	0.090	0.060	0.120			
4	0.160	0.080	0.200	83.51	13.57	2.92
5	0.260	0.120	0.320	81.15	15.58	3.27
6	0.400	0.160	0.480	86.62	11.16	2.22
7	0.580	0.200	0.680	78.73	18.06	3.21
8	0.800	0.240	0.920	88.12	8.98	2.90
9	1.060	0.280	1.200	95.00	3.00	2.00
10	1.360	0.320	1.520			
11	1.700	0.360	1.880	92.50	4.00	3.50
12	2.080	0.400	2.280	90.00	5.00	5.00
13	2.500	0.440	2.720			
14	2.990	0.540	3.260			
15	3.580	0.640	3.900			
16	4.270	0.740	4.640	68.00	20.00	12.00
17	5.060	0.840	5.480			
18	5.950	0.940	6.420			
19	6.940	1.040	7.460			
20	7.980	1.040	8.500			

Layer node depth ( $Z_i$ ), thickness ( $\Delta Z_i$ ), and depth at layer interface ( $Z_{h,i}$ ) for default soil column. All in meters.

Accordingly, we revised the sentences in lines 174-186 as "The soil hydraulic parameters, including the porosity, saturated hydraulic conductivity, hydraulic potential, the Clapp-Hornberger parameter  $b$ , field capacity, wilt point, and saturated soil water diffusivity, were determined using the pedotransfer functions proposed by Hillel (1980), Cosby et al. (1984), and Wetzels and Chang (1987) (Equations S1-S7), in which the sand and clay percentages were based on Hu et al., (2017) (Table S1). In addition, the simulation depth was extended to 8.0 m to cover the active layer thickness of the QTP. The soil column was discretized into 20 layers, whose depths follow the default scheme in CLM 5.0 (Table S1, Lawrence et al., 2018). Due to the inexact match between observed and simulated depths, the simulations at 4cm, 26cm, 80cm, 136cm, 208cm and 299cm were compared with the observations at 5cm, 25cm, 70cm, 140cm, 220cm and 300cm, respectively. A 30-year spin-up was conducted in every simulation to reach equilibrium soil states."

3. Line 189: What is “Si”?

**Response:** Sorry for the typo. It should be  $\overline{\Delta RMSE}$ , which has been corrected in line 203.

4. What is the model timestep in the simulations in this study?

**Response:** The model was driven by 1-hr-interval atmospheric forcing data, which has been described in lines 138-144: "The atmospheric forcing data, including wind speed/direction, air temperature/relative humidity/pressure, downward shortwave/longwave radiation, and precipitation, were used to drive the model. These variables above were measured at a height of 2 m and covered the period from August 10, 2010 to August 10, 2012 (Beijing time) with a temporal resolution of 1 hour. Daily soil temperature and moisture at depths of 5cm, 25cm, 70cm, 140cm, 220cm and 300cm from October 1, 2010 to September 30, 2011 (Beijing time) were utilized to validate the simulation results."

5. Section 4.3: The authors only tested the model performance at one site. So to what extent their conclusions can be extended to other Tibetan Plateau areas?

**Response:** Thanks for this review. We agree that further work is required in the future as discussed in Sec. 4.4. In this study, our main goal is to provide a reference for simulating permafrost state on the Tibet Plateau. However, before the whole Tibetan Plateau can be investigated, it is necessary to conduct such study at the site scale.

We believe the conclusion of the cold bias of Noah-MP in the Tibetan Plateau and the possible reasons are of high reliability. The study site is a typical permafrost site on the plateau with semiarid climate (Li et al., 2019), filmy and discontinuous snow cover (Che et al., 2019), sparse grassland (Yao et al., 2011), coarse soil (Wu and Nan, 2016; He et al., 2019), and thick active layer (Luo et al., 2016), which are common features in the permafrost regions of the plateau. In addition, such underestimations and the inabilities of producing the snow depth, diurnal  $Z_{0h}$  and frozen soil thermal conductivity

are widely reported in many state-of-the-art land surface models as discussed in Sec. 4.1 and 4.2.

In addition, the sensitivity analysis and optimal configuration of the physical processes in this study could contribute to better understand the land surface processes and provide practical guidelines for permafrost modeling at least in the permafrost areas with similar conditions on the plateau. Relevant methodologies could be generalized to other regions using the proposed approaches.

To be more unbiased and objective, we added some descriptions about the study site, and the new version in lines 126-131 are: "Tanggula observation station (TGL) lies in the continuous permafrost regions of Tanggula Mountain, central QTP (33.07°N, 91.93°E, Alt.: 5,100 m a.s.l; Fig. 1). This site a typical permafrost site on the plateau with sub-frigid and semiarid climate (Li et al., 2019), filmy and discontinuous snow cover (Che et al., 2019), sparse grassland (Yao et al., 2011), coarse soil (Wu and Nan, 2016; He et al., 2019), and thick active layer (Luo et al., 2016), which are common features in the permafrost regions of the plateau."

And the perspective part (section 4.4) in lines 603-612 are rephrased as: "This study analyzed the characteristics and general behaviors of each parameterization scheme of Noah-MP at a typical permafrost site on the QTP, hoping to provide a reference for simulating permafrost state on the QTP. We identified the systematic overestimation of snow cover and cold bias in Noah-MP, and discussed the possible sources of error. Relevant results and methodologies can be practical guidelines for improving the parameterizations of physical processes and testing their uncertainties towards near-surface permafrost modeling on the plateau. Although the site we selected may be representative for the typical environment on the plateau, continued investigation with a broad spectrum of climate and environmental conditions is required to make a general conclusion at regional scale."

### Other changes:

- Thanks to the funded projects and referees in lines 683-688: "This work has been supported by the CAS "Light of West China" Program, and the National Natural Science Foundation of China (41690142; 41771076; 41961144021; 41671070). The authors thank Cryosphere Research Station on the Qinghai-Tibet Plateau, CAS for providing field observation data used in this study. We would like to thank two anonymous reviewers for their insightful and constructive comments and suggestions, which greatly improved the quality of the manuscript."
- We have rerun the simulations involving RUN(3) as replied to the comment #3 from referee #2, and all the figures in the manuscript have been revised accordingly.
- All the unfrozen water in the manuscript have been revised as soil liquid water (SLW).
- Delete "under review" in line 161
- Rewrite the sentences in lines 193-196 as: "The root mean square error (RMSE) between the simulations and observations were adopted to evaluate the performance of Noah-MP. The average of the RMSEs of all the soil layers was defined as column RMSE (colRMSE)."
- The study of Li et al. (2015) is cited in line 200:  
Li, K., Gao, Y., Fei, C., Xu, J., Jiang, Y., Xiao, L., Li, R., and Pan, Y.: Simulation of impact of roots on soil moisture and surface fluxes over central Qinghai – Xizang Plateau. *Plateau Meteor.*, 34, 642-652, <https://doi.org/10.7522/j.issn.1000-0534.2015.00035>, 2015.
- Delete the interaction analysis part in lines 328-346

### References:

- Che, T., Hao, X., Dai, L., Li, H., Huang, X., and Xiao, L.: Snow cover variation and its impacts over the Qinghai-Tibet Plateau, *Bull. Chin. Acad. Sci.*, 34, 1247-1253, <https://doi.org/10.16418/j.issn.1000-3045.2019.11.007>, 2019.
- He, K., Sun, J., and Chen, Q.: Response of climate and soil texture to net primary productivity and precipitation-use efficiency in the Tibetan Plateau, *Pratacultural Science*, 36(4), 1053–1065. <https://doi.org/10.11829/j.issn.1001-0629.2019-0036>, 2019.
- Li, R., Zhao, L., Wu, T., Wang, Q. X., Ding, Y., Yao, J., Wu, X., Hu, G., Xiao, Y., Du, Y., Zhu, X., Qin, Y., Shuhua, Y., Bai, R., Erji, D., Liu, G., Zou, D., Yongping, Q., and Shi, J.: Soil thermal conductivity and its influencing factors at the Tanggula permafrost region on the Qinghai–Tibet Plateau, *Agric. For. Meteor.*,

264, 235-246, <https://doi.org/10.1016/j.agrformet.2018.10.011>, 2019.

Luo, D., Wu, Q., Jin, H., Marchenko, S., Lyu, L., and Gao, S.: Recent changes in the active layer thickness across the northern hemisphere, *Environ. Earth Sci.*, 75(7), 555. <https://doi.org/10.1007/s12665-015-5229-2>, 2016.

Wu, X., and Nan, Z.: A multilayer soil texture dataset for permafrost modeling over Qinghai-Tibetan Plateau. Paper presented at 2016 IEEE International Geoscience and Remote Sensing Symposium (IGARSS), Beijing, China. <https://doi.org/10.1109/IGARSS.2016.7730283>, 2016.

Yao, J., Zhao, L., Gu, L., Qiao, Y., and Jiao, K.: The surface energy budget in the permafrost region of the Tibetan Plateau, *Atmos. Res.*, 102, 394-407, <https://doi.org/https://doi.org/10.1016/j.atmosres.2011.09.001>, 2011.

## Responses to Referee #2

### Anonymous Referee #2

Received and published: 13 October 2020

It's my pleasure to review gmd-2020-142 "Assessing the simulated soil thermal regime from Noah-MP LSM v1.1 for near-surface permafrost modeling on the Qinghai-Tibet Plateau" by Li et al. The authors evaluate the performance of Noah-MP in simulating soil temperature on a permafrost site over the Tibetan Plateau. There are many additional work need to be done before this paper can be accepted.

1. I note that there is a paper recently published by the same author to improve the performance of Noah-MP simulations on the same site. It will be interesting the authors firstly add their improvements, and then design more numerical experiments to test the uncertainties of different parameterization options.

**Response:** Thanks for this comment. The recently published work you mentioned only tested and augmented one selected combination of Noah-MP options. However, this study investigated the general performance and sensitivity of original Noah-MP model with all possible combinations, hoping to provide a reference for simulating permafrost state on the Tibet Plateau. The augmentation work is another big issue and out of scope of this paper. We choose not to add the suggested experiments, but highlight the continued efforts to augment the parameterizations of physical processes and test their uncertainties in the future in lines 603-612:

"This study analyzed the characteristics and general behaviors of each parameterization scheme of Noah-MP at a typical permafrost site on the QTP, hoping to provide a reference for simulating permafrost state on the QTP. We identified the systematic overestimation of snow cover and cold bias in Noah-MP, and discussed the possible sources of error. Relevant results and methodologies can be practical guidelines for improving the parameterizations of physical processes and testing their uncertainties towards near-surface permafrost modeling on the plateau. Although the site we selected may be representative for the typical environment on the plateau, continued



investigation with a broad spectrum of climate and environmental conditions is required to make a general conclusion at regional scale."

With these revisions, we believe the potential readers can understand that our study aims to test the performance of the original Noah-MP, while future work is needed at the plateau scale.

Since one additional site, soil moisture and snow measurements are available, the authors are suggested to also use these measurements to test the Noah-MP's performance. For the frozen soil, the soil moisture and soil temperature are fully coupled, which are also affected by the snow process, so it's also important to evaluate the performance of Noah-MP in simulating these variables.

**Response:** We agree that add more sites would strengthen our conclusions. However, we realized that this will make our manuscript very long, and it is difficult to describe the results due to the different environmental factors among the sites. Our main goal is to provide a reference for simulating permafrost state on the Tibet Plateau. We tried our best to make this manuscript concise. Therefore, we would rather focus on one site, and it would be easier for potential readers to understand the core ideas.

We realized that potential readers may wonder why we did not assess the model using more data. To be clear, we explained this in the revised version in lines 603-612 as follows: "This study analyzed the characteristics and general behaviors of each parameterization scheme of Noah-MP at a typical permafrost site on the QTP, hoping to provide a reference for simulating permafrost state on the QTP. We identified the systematic overestimation of snow cover and cold bias in Noah-MP, and discussed the possible sources of error. Relevant results and methodologies can be practical guidelines for improving the parameterizations of physical processes and testing their uncertainties towards near-surface permafrost modeling on the plateau. Although the site we selected may be representative for the typical environment on the plateau, continued investigation with a broad spectrum of climate and environmental conditions

is required to make a general conclusion at regional scale."

To be more unbiased and objective, we added more descriptions about the study site, in lines 126-131: "Tanggula observation station (TGL) lies in the continuous permafrost regions of Tanggula Mountain, central QTP (33.07°N, 91.93°E, Alt.: 5,100 m a.s.l; Fig. 1). This site a typical permafrost site on the plateau with sub-frigid and semiarid climate (Li et al., 2019), filmy and discontinuous snow cover (Che et al., 2019), sparse grassland (Yao et al., 2011), coarse soil (Wu and Nan, 2016; He et al., 2019), and thick active layer (Luo et al., 2016), which are common features in the permafrost regions of the plateau."

With these revisions, we believe the potential readers can understand our main findings. We keep the manuscript not too lengthy.

- About snow

As the reply to Referee #1, we conducted 41472 simulations to test the performance of Noah-MP in simulating snow cover. Similar with the recently published paper you mentioned (Li et al., 2020), ground albedo was used to roughly reflect the snow events. Our results show that Noah-MP extremely overestimates the albedo and thus induces great cold bias in soil temperature. Detailed results and discussions are illustrated in the newly added Sec. 3.1.1 and Sec. 4.1, respectively.

- About soil moisture

We checked the performance of Noah-MP in simulating soil liquid water (SLW) in the revised manuscript. Results show that the Noah-MP model generally underestimates soil moisture across the profile. The RUN process dominates the SLW simulation in comparison of the very limited impacts of all other physical processes. Detailed results can be found in lines Sec. 3.1.2 and Sec. 3.2.2.

2. Since the snow process is also important for permafrost soil temperature simulations,

it's suggested to also consider the impact of ALB and SNF options.

**Response:** In the revised manuscript, we firstly checked the performance of Noah-MP for snow simulation and its impacts on soil temperature by considering the ALB and SNF options. Results showed that Noah-MP greatly overestimates snow cover both in magnitude and duration, inducing huge cold bias and large uncertainties in soil temperatures. However, our in-situ measurements and other studies show that snow cover has a very limited influence on soil temperature. Given the poor simulation of Noah-MP for snow cover and the weak impact of snow on soil temperature in reality, we did not consider the snow process in the following parts.

Detailed results and discussions are illustrated in the newly added Sec. 3.1.1 and Sec. 4.1, respectively.

3. It's also suggested to evaluate the performance of Noah-MP for frozen (e.g. October-April) and thawed (e.g. May-September) soil conditions separately. Because it's very strange to me that the impact of RUN is so important for the soil temperature simulations.

**Response:** We firstly apologize for the wrong coding when modifying the default Noah-MP to consider the vertical heterogeneity in the soil profile. In the wrong version, the maximum infiltration rate in RUN(3) was calculated as a function of all the soil layers (up to 8m in this study). Due to the existence of permafrost below 3m at the study site, the calculated infiltration rate is extremely small, resulting in small soil moisture of RUN(3) (Figure S1 in previous manuscript) and thus great influence degree of RUN process (Figure 3 in previous manuscript).

Following the default Noah-MP, we have rewritten the infiltration rate in RUN(3) as a function of the soil layers no more than 2m. Based on this, we reassessed the performance of Noah-MP for frozen and thawed soil conditions.

However, the main conclusion is consistent with previous manuscript except the

declined influence of RUN process on soil temperature simulation. We have rewritten the main conclusions in lines 640-659 as:

- (1) "Noah-MP model tends to overestimate snow cover and thus largely underestimate soil temperature in the permafrost regions of the QTP. Systematic cold bias and large uncertainties of soil temperature still exist after removing the snow processes, particularly at the deep layers and during the cold season. This is largely due to the imperfect model structure with regard to the roughness length for heat and soil thermal conductivity.
- (2) Soil temperature is dominated by the surface layer drag coefficient (SFC) while largely influenced by runoff and groundwater (RUN). Other physical processes have little impact on ST simulation, among which VEG, RAD, and STC are more influential on shallow ST, while FRZ, INF and TBOT have greater impacts on deep ST. In addition, CRS and BTR do not significantly affect the simulation results.
- (3) The best scheme combination for permafrost simulation are as follows: VEG (table LAI, calculated vegetation fraction), CRS (Jarvis), BTR (Noah), RUN (BATS), SFC (Chen97), RAD (zero canopy gap), FRZ (variant freezing-point depression), INF (hydraulic parameters defined by soil moisture), TBOT (ST at 8 m), STC (semi-implicit)."

4. Detailed information is needed for the following descriptions "The soil 164 hydraulic parameters, including the porosity, saturated hydraulic conductivity, hydraulic potential, the Clapp-Hornberger parameter  $b$ , field capacity, wilt point, and saturated soil water diffusivity, were determined using the pedotransfer functions proposed by Hillel (1980), Cosby et al. (1984), and Wetzel and Chang (1987), in which the sand and clay percentages were based on Hu et al., (2017). In addition, the simulation depth was extended to 8.0 m to cover the active layer thickness of the QTP. The soil column was discretized following the default scheme in CLM 5.0 (Lawrence et al., 2018)."

**Response:** We have added the details of the pedotransfer functions, the discretization scheme of soil column, and the soil particle fractions in the supplementary file:

The soil hydraulic parameters of each layer, including the porosity ( $\theta_s$ ), saturated hydraulic conductivity ( $K_s$ ), hydraulic potential ( $\psi_s$ ), the Clapp-Hornberger parameter ( $b$ ), field capacity ( $\theta_{ref}$ ), wilt point ( $\theta_w$ ), and saturated soil water diffusivity ( $D_s$ ), were determined using the pedotransfer functions proposed by Hillel (1980), Cosby et al. (1984), and Wetzels and Chang (1987):

$$\theta_s = 0.489 - 0.00126(\%sand) \quad (S1)$$

$$K_s = 7.0556 \times 10^{-6.884+0.0153(\%sand)} \quad (S2)$$

$$\psi_s = -0.01 \times 10^{1.88-0.0131(\%sand)} \quad (S3)$$

$$b = 2.91 + 0.159(\%clay) \quad (S4)$$

$$\theta_{ref} = \theta_s \left[ \frac{1}{3} + \frac{2}{3} \left( \frac{5.79 \times 10^{-9}}{K_s} \right)^{1/(2b+3)} \right] \quad (S5)$$

$$\theta_w = 0.5\theta_s \left( \frac{-200}{\psi_s} \right)^{-1/b} \quad (S6)$$

$$D_s = b \cdot K_s \cdot \left( \frac{\psi_s}{\theta_s} \right) \quad (S7)$$

where *%sand* and *%clay* represent the percentage (%) of sand and clay content in soil, respectively.

**Table S1** Soil discretization scheme and soil particle fraction in this study.

Layer	Z <sub>i</sub>	ΔZ <sub>i</sub>	Z <sub>h,i</sub>	Sand (%)	Silt (%)	Clay (%)
1	0.010	0.020	0.020	85.48	12.59	1.93
2	0.040	0.040	0.060			
3	0.090	0.060	0.120			
4	0.160	0.080	0.200	83.51	13.57	2.92
5	0.260	0.120	0.320	81.15	15.58	3.27
6	0.400	0.160	0.480	86.62	11.16	2.22
7	0.580	0.200	0.680	78.73	18.06	3.21
8	0.800	0.240	0.920	88.12	8.98	2.90
9	1.060	0.280	1.200	95.00	3.00	2.00
10	1.360	0.320	1.520			
11	1.700	0.360	1.880	92.50	4.00	3.50
12	2.080	0.400	2.280	90.00	5.00	5.00
13	2.500	0.440	2.720			
14	2.990	0.540	3.260			
15	3.580	0.640	3.900			
16	4.270	0.740	4.640	68.00	20.00	12.00
17	5.060	0.840	5.480			

18	5.950	0.940	6.420			
19	6.940	1.040	7.460			
20	7.980	1.040	8.500			

Layer node depth ( $Z_i$ ), thickness ( $\Delta Z_i$ ), and depth at layer interface ( $Z_{h,i}$ ) for default soil column. All in meters.

Accordingly, we revised the sentences in lines 174-186 as "The soil hydraulic parameters, including the porosity, saturated hydraulic conductivity, hydraulic potential, the Clapp-Hornberger parameter  $b$ , field capacity, wilt point, and saturated soil water diffusivity, were determined using the pedotransfer functions proposed by Hillel (1980), Cosby et al. (1984), and Wetzels and Chang (1987) (Equations S1-S7), in which the sand and clay percentages were based on Hu et al., (2017) (Table S1). In addition, the simulation depth was extended to 8.0 m to cover the active layer thickness of the QTP. The soil column was discretized into 20 layers, whose depths follow the default scheme in CLM 5.0 (Table S1, Lawrence et al., 2018). Due to the inexact match between observed and simulated depths, the simulations at 4cm, 26cm, 80cm, 136cm, 208cm and 299cm were compared with the observations at 5cm, 25cm, 70cm, 140cm, 220cm and 300cm, respectively. A 30-year spin-up was conducted in every simulation to reach equilibrium soil states."

#### **Other changes:**

- Thanks to the funded projects and referees in lines 683-688: "This work has been supported by the CAS "Light of West China" Program, and the National Natural Science Foundation of China (41690142; 41771076; 41961144021; 41671070). The authors thank Cryosphere Research Station on the Qinghai-Tibet Plateau, CAS for providing field observation data used in this study. We would like to thank two anonymous reviewers for their insightful and constructive comments and suggestions, which greatly improved the quality of the manuscript."
- We have rerun the simulations involving RUN(3) as replied to the comment #3 from referee #2, and all the figures in the manuscript have been revised accordingly.
- All the unfrozen water in the manuscript have been revised as soil liquid water (SLW).
- Delete "under review" in line 161
- Rewrite the sentences in lines 193-196 as: "The root mean square error (RMSE) between the simulations and observations were adopted to evaluate the

performance of Noah-MP. The average of the RMSEs of all the soil layers was defined as column RMSE (colRMSE)."

- The study of Li et al. (2015) is cited in line 200:

Li, K., Gao, Y., Fei, C., Xu, J., Jiang, Y., Xiao, L., Li, R., and Pan, Y.: Simulation of impact of roots on soil moisture and surface fluxes over central Qinghai – Xizang Plateau. *Plateau Meteor.*, 34, 642-652, <https://doi.org/10.7522/j.issn.1000-0534.2015.00035>, 2015.

- Delete the interaction analysis part in lines 328-346

1 **Assessing the simulated soil thermal regime from Noah-MP LSM**  
2 **v1.1 for near-surface permafrost modeling on the Qinghai-Tibet**  
3 **Plateau**

4

5 Xiangfei Li<sup>1,2</sup>, Tonghua Wu<sup>1,\*</sup>, Xiaodong Wu<sup>1</sup>, Xiaofan Zhu<sup>1</sup>, Guojie Hu<sup>1</sup>, Ren Li<sup>1</sup>,  
6 Yongping Qiao<sup>1</sup>, Cheng Yang<sup>1,2</sup>, Junming Hao<sup>1,2</sup>, Jie Ni<sup>1,2</sup>, Wensi Ma<sup>1,2</sup>

7

8 <sup>1</sup> Cryosphere Research Station on the Qinghai-Tibet Plateau, State Key Laboratory of  
9 Cryospheric Science, Northwest Institute of Eco-Environment and Resources, Chinese  
10 Academy of Sciences, Lanzhou 730000, China

11 <sup>2</sup>University of Chinese Academy of Sciences, Beijing 100049, China

12

13 **Correspondence:** Tonghua Wu (thuawu@lzb.ac.cn)

14



15 **Abstract.** Land surface models (LSMs) are effective tools for near-surface permafrost  
16 modeling. Extensive and rigorous model inter-comparison is of great importance before  
17 application due to the uncertainties in current LSMs. This study designed an ensemble  
18 of 6912 experiments to evaluate the Noah land surface model with multi-  
19 parameterization (Noah-MP) for soil temperature (ST) and soil liquid water (SLW)  
20 simulation, and investigate the sensitivity of parameterization schemes at a typical  
21 permafrost site on the Qinghai-Tibet Plateau. The results showed that Noah-MP  
22 systematically overestimates snow cover and thus induces great cold bias in ST. After  
23 removing the snow process, Noah-MP generally underestimates STthe cold bias remain,  
24 especially ~~that~~ during the cold season. ~~In addition, And~~ ~~the simulation~~ uncertainty of ST  
25 is greater in the cold season (October-April) and for the deep soil layers. ST is most  
26 sensitive to surface layer drag coefficient (SFC) while largely influenced by runoff and  
27 groundwater (RUN). By contrast, the influence of canopy stomatal resistance (CRS)  
28 and soil moisture factor for stomatal resistance (BTR) on ST is negligible. With limited  
29 impacts on ST simulation, vegetation model (VEG), canopy gap for radiation transfer  
30 (RAD) and snow/soil temperature time scheme (STC) are more influential on shallow  
31 ST, while super-cooled liquid water (FRZ), frozen soil permeability (INF) and lower  
32 boundary of soil temperature (TBOT) have greater impacts on deep ST. In addition,  
33 Noah-MP generally underestimates soil moisture. The RUN process dominates the  
34 SLW simulation in comparison of the very limited impacts of all other physical  
35 processes. Furthermore, an optimal configuration of Noah-MP for permafrost modeling  
36 were extracted based on the connectivity between schemes, and they are: table leaf area  
37 index with calculated vegetation fraction, Jarvis scheme for CRS, Noah scheme for  
38 BTR, BATS model for RUN, Chen97 for SFC, zero canopy gap for RAD, variant  
39 freezing-point depression for FRZ, hydraulic parameters defined by soil moisture for  
40 INF, ST at 8 m for TBOT, and semi-implicit method for STC. The analysis of the model  
41 structural uncertainties and characteristics of each scheme would be constructive to a  
42 better understanding of the land surface processes on the QTP and further model  
43 improvements towards near-surface permafrost modeling using the LSMs.

44

## 45 **1 Introduction**

46 The Qinghai-Tibet Plateau (QTP) hosts the world's largest high-altitude  
47 permafrost covering a contemporary area of  $1.06 \times 10^6$  km<sup>2</sup> (Zou et al., 2017). Under  
48 the background of climate warming and intensifying human activities, permafrost on  
49 the QTP has been widely suffering thermal degradation (Ran et al., 2018), resulting in  
50 reduction of permafrost extent, disappearing of permafrost patches and thickening of  
51 active layer (Chen et al., 2020). Moreover, such degradation could cause alterations in  
52 hydrological cycles (Zhao et al., 2019; Woo, 2012), changes on ecosystem (Fountain et  
53 al., 2012; Yi et al., 2011) and damages to infrastructures (Hjort et al., 2018). Therefore,  
54 it is very important to monitor and simulate the state of permafrost to adapt to the  
55 degradation.

56 Soil temperature (ST) is an intuitive indicator to evaluate the thermal state of  
57 permafrost. A number of monitoring sites have been established on the QTP (Cao et al.,  
58 2019). However, it is inadequate to construct the thermal state of permafrost by  
59 considering the spatial variability of the ground thermal regime and an uneven  
60 distribution of these observations. In contrast, numerical models are competent  
61 alternatives. In recent years, land surface models (LSMs), which describe the exchanges  
62 of heat, water, and momentum between the land and atmosphere (Maheu et al., 2018),  
63 have received significant improvements in the representation of permafrost and frozen  
64 ground processes (Koven et al., 2013; Nicolsky et al., 2007; Melton et al., 2019). LSMs  
65 are capable of simulating the transient change of permafrost by describing subsurface  
66 hydrothermal processes (e.g. soil temperature and moisture) with soil heat conduction  
67 (-diffusion) and water movement equations (Daniel et al., 2008). Moreover, they can  
68 be integrated with the numerical weather prediction system like WRF (Weather  
69 Research and Forecasting), making them as effective tools for comprehensive  
70 interactions between climate and permafrost (Nicolsky et al., 2007).

71 Some LSMs have been applied to modeling permafrost in the QTP. Guo and Wang  
72 (2013) investigated near-surface permafrost and seasonally frozen ground states as well  
73 as their changes using the Community Land Model, version 4 (CLM4). Hu et al. (2015)

74 applied the coupled heat and mass transfer model to identify the hydrothermal  
75 characteristics of the permafrost active layer in the Qinghai-Tibet Plateau. Using an  
76 augmented Noah LSM, Wu et al. (2018) modeled the extent of permafrost, active layer  
77 thickness, mean annual ground temperature, depth of zero annual amplitude and ground  
78 ice content on the QTP in 2010s. Despite those achievements based on different models,  
79 LSMs are in many aspects insufficient for permafrost modeling. For one thing, large  
80 uncertainties still exist in the state-of-the-art LSMs when simulating the soil  
81 hydrothermal regime on the QTP (Chen et al., 2019). For instance, 19 LSMs in CMIP5  
82 overestimate snow depth over the QTP (Wei and Dong, 2015), which could result in the  
83 variations of the soil thermal regime in the aspects of magnitude and vector (cooling or  
84 warming) (Zhang, 2005). Moreover, most of the existing LSMs are not originally  
85 developed for permafrost modeling. Many of their soil processes are designed for  
86 shallow soil layers (Westermann et al., 2016), but permafrost may occur in the deep  
87 soil. And the soil column is often considered homogeneous, which can not represent  
88 the stratified soil common on the QTP (Yang et al., 2005). Given the numerous LSMs  
89 and possible deficiencies, it is necessary to assess the parameterization schemes for  
90 permafrost modeling on the QTP, which is helpful to identify the influential sub-  
91 processes, enhance our understanding of model behavior, and guide the improvement  
92 of model physics (Zhang et al., 2016).

93 Noah land surface model with multi-parameterization (Noah-MP) provides a  
94 unified framework in which a given physical process can be interpreted using multiple  
95 optional parameterization schemes (Niu et al., 2011). Due to the simplicity in selecting  
96 alternative schemes within one modeling framework, it has been attracting increasing  
97 attention in inter-comparison work among multiple parameterizations at point and  
98 watershed scales (Hong et al., 2014; Zheng et al., 2017; Gan et al., 2019; Zheng et al.,  
99 2019; Chang et al., 2020; You et al., 2020). For example, Gan et al. (2019) carried an  
100 ensemble of 288 simulations from multi-parameterization schemes of six physical  
101 processes, assessed the uncertainties of parameterizations in Noah-MP, and further  
102 revealed the best-performing schemes for latent heat, sensible heat and terrestrial water

103 storage simulation over ten watersheds in China. You et al. (2020) assessed the  
104 performance of Noah-MP in simulating snow process at eight sites over distinct snow  
105 climates and identified the shared and specific sensitive parameterizations at all sites,  
106 finding that sensitive parameterizations contribute most of the uncertainties in the  
107 multi-parameterization ensemble simulations. Nevertheless, there is little research on  
108 the inter-comparison of soil thermal processes toward permafrost modeling. In this  
109 study, an ensemble experiment of totally 6912 scheme combinations was conducted at  
110 a typical permafrost monitoring site on the QTP. The simulated soil temperature (ST)  
111 of Noah-MP model was assessed and the sensitivities of parameterization schemes at  
112 different depths were further investigated. Considering the general performance and  
113 sensitive schemes of Noah-MP, we further explored the interactions between the most  
114 influential schemes and configured an optimal combination based on the connections  
115 between schemes. We hope this study can provide a reference for permafrost simulation  
116 on the QTP.

117 This article is structured as follows: Section 2 introduces the study site,  
118 atmospheric forcing data, design of ensemble simulation experiments, and sensitivity  
119 analysis and optimal selection methods. Section 3 describes the ensemble simulation  
120 results of ST, explores the sensitivity and interactions of parameterization schemes, and  
121 determines the optimal combination for permafrost modeling. Section 4 discusses the  
122 schemes in each physical process and proposes further research topics. Section 5  
123 concludes the main findings of this study.

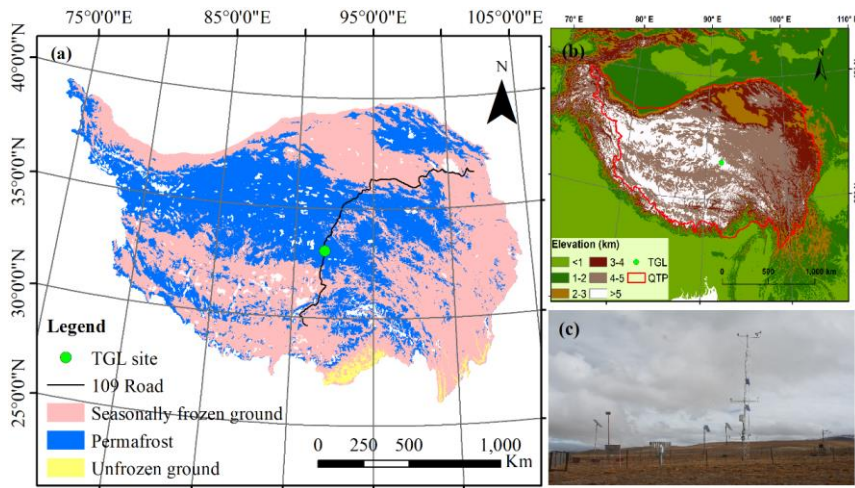
## 124 **2 Methods and materials**

### 125 **2.1 Site description and observation datasets**

126 Tanggula observation station (TGL) lies in the continuous permafrost regions of  
127 Tanggula Mountain, central QTP (33.07°N, 91.93°E, Alt.: 5,100 m a.s.l; Fig. 1). This  
128 site [a typical permafrost site on the plateau with sub-frigid and semiarid climate \(Li et](#)  
129 [al., 2019\), filmy and discontinuous snow cover \(Che et al., 2019\), sparse grassland \(Yao](#)

130 [et al., 2011](#)), coarse soil ([Wu and Nan, 2016](#); [He et al., 2019](#)), and thick active layer  
 131 ([Luo et al., 2016](#)), which are common features in the permafrost regions of the plateau, is  
 132 characterized by the sub-frigid and semiarid climate ([Li et al., 2019](#)). According to the  
 133 observations from 2010–2011, the annual mean air temperature of TGL site was  
 134  $-4.4\text{ }^{\circ}\text{C}$ . The annual precipitation was 375 mm, and of which 80% is concentrated  
 135 between May and September. Alpine steppe with low height is the main land surface,  
 136 whose coverage range is about 40% ~ 50% ([Yao et al., 2011](#)). The active layer thickness  
 137 is about 3.15 m ([Hu et al., 2017](#)).

138 The atmospheric forcing data, including wind speed/direction, air  
 139 temperature/relative humidity/pressure, downward shortwave/longwave radiation, and  
 140 precipitation, were used to drive the model. These variables above were measured at a  
 141 height of 2 m and covered the period from August 10, 2010 to August 10, 2012 (Beijing  
 142 time) with a temporal resolution of 1 hour. Daily soil temperature [and liquid moisture](#)  
 143 [at depths of 5cm, 25cm, 70cm, 140cm, 220cm and 300cm](#) from October 1, 2010 to  
 144 September 30, 2011 (Beijing time) were utilized to validate the simulation results.



145  
 146 **Figure 1.** Location and geographic features of study site. (a) Location of observation  
 147 site and permafrost distribution ([Zou et al., 2017](#)). (b) Topography of the Qinghai-Tibet  
 148 Plateau. (c) Photo of the Tanggula observation station.

## 149 2.2 Ensemble experiments of Noah-MP

150 The offline Noah-MP LSM v1.1 was assessed in this study. It consists of 12  
151 physical processes that are interpreted by multiple optional parameterization schemes.  
152 These sub-processes include vegetation model (VEG), canopy stomatal resistance  
153 (CRS), soil moisture factor for stomatal resistance (BTR), runoff and groundwater  
154 (RUN), surface layer drag coefficient (SFC), super-cooled liquid water (FRZ), frozen  
155 soil permeability (INF), canopy gap for radiation transfer (RAD), snow surface albedo  
156 (ALB), precipitation partition (SNF), lower boundary of soil temperature (TBOT) and  
157 snow/soil temperature time scheme (STC) (Table 1). Details about the processes and  
158 optional parameterizations can be found in Yang et al. (2011a).

159 In this study, the dynamic vegetation option in VEG process was turned off for  
160 simplicity. Previous studies has confirmed that Noah-MP seriously overestimate the  
161 snow depth on the QTP (Li et al., 2020-(under review); Wang et al., 2020). However,  
162 the impact of snow cover on ground temperatures in the permafrost regions of QTP is  
163 usually considered weak (Jin et al., 2008; Wu et al., 2018), because the snow cover is  
164 thin, short-lived, and patchy-distributed (Che et al., 2019). For practical purpose  
165 to avoid the possible bias caused by snow process, the ALB and SNF processes were not  
166 considered by setting the snow fraction in precipitation to zero. Since no snow cover in  
167 the ground, the ground albedo equals the soil albedo. As a result, in total 6912  
168 combinations are possible for the left 10 processes and orthogonal experiments were  
169 carried out to evaluate their performance in soil thermal dynamics and obtain the  
170 optimal combination.

171 The monthly leaf area index (LAI) was derived from the Advanced Very High-  
172 Resolution Radiometer (AVHRR) (<https://www.ncei.noaa.gov/data/>, Claverie et al.,  
173 2016). The Noah-MP model was modified to consider the vertical heterogeneity in the  
174 soil profile by setting the corresponding soil parameters for each layer. The soil  
175 hydraulic parameters, including the porosity, saturated hydraulic conductivity,  
176 hydraulic potential, the Clapp-Hornberger parameter b, field capacity, wilt point, and  
177 saturated soil water diffusivity, were determined using the pedotransfer functions

178 proposed by Hillel (1980), Cosby et al. (1984), and Wetzel and Chang (1987)  
 179 ([Equations S1-S7](#)), in which the sand and clay percentages were based on Hu et al.,  
 180 (2017) ([Table S1](#)). In addition, the simulation depth was extended to 8.0 m to cover the  
 181 active layer thickness of the QTP. The soil column was discretized [into 20 layers, whose](#)  
 182 [depths following the default scheme in CLM 5.0 \(Table S1, Lawrence et al., 2018\). Due](#)  
 183 [to the inexact match between observed and simulated depths, the simulations at 4cm,](#)  
 184 [26cm, 80cm, 136cm, 208cm and 299cm were compared with the observations at 5cm,](#)  
 185 [25cm, 70cm, 140cm, 220cm and 300cm, respectively.](#) A 30-year spin-up was conducted  
 186 in every simulation to reach equilibrium soil states.

187 **Table 1.** The physical processes and options of Noah-MP. Options in bold are the  
 188 optimal selections in this study.

Physical processes	Options
Vegetation model (VEG)	(1) table LAI, prescribed vegetation fraction (2) dynamic vegetation <b>(3) table LAI, calculated vegetation fraction</b> (4) table LAI, prescribed max vegetation fraction
Canopy stomatal resistance (CRS)	<b>(1) Jarvis</b> (2) Ball-Berry
Soil moisture factor for stomatal resistance (BTR)	<b>(1) Noah</b> (2) CLM (3) SSiB
Runoff and groundwater (RUN)	(1) SIMGM with groundwater (2) SIMTOP with equilibrium water table (3) Noah (free drainage) <b>(4) BATS (free drainage)</b>
Surface layer drag coefficient (SFC)	(1) Monin-Obukhov (M-O) <b>(2) Chen97</b>
Super-cooled liquid water (FRZ)	(1) generalized freezing-point depression <b>(2) Variant freezing-point depression</b>
Frozen soil permeability (INF)	<b>(1) Defined by soil moisture, more permeable</b> (2) Defined by liquid water, less permeable
Canopy gap for radiation transfer (RAD)	(1) Gap=F(3D structure, solar zenith angle) <b>(2) Gap=zero</b> (3) Gap=1-vegetated fraction
Snow surface albedo (ALB)	(1) BATS (2) CLASS
Precipitation partition (SNF)	(1) Jordan91 (2) BATS: $T_{sfc} < T_{fz} + 2.2K$ (3) $T_{sfc} < T_{fz}$

Lower boundary of soil temperature (TBOT)	(1) zero heat flux (2) soil temperature at 8m depth
Snow/soil temperature time scheme (STC)	(1) semi-implicit (2) full implicit

189 BATS (Biosphere–Atmosphere Transfer Model); CLASS (Canadian Land Surface Scheme);  
 190 SIMGM (Simple topography-based runoff and Groundwater Model); SIMTOP (Simple  
 191 Topography-based hydrological model); SSiB (Simplified Simple Biosphere model).

### 192 2.3 Methods for sensitivity analysis

193 The root mean square error (RMSE) ~~and standard deviation (SD)~~ between the  
 194 simulations and observations were adopted to evaluate the performance of Noah-MP.  
 195 The averages of the RMSEs ~~and SDs~~ of all the soil layers were defined as column  
 196 RMSE (colRMSE) ~~and column SD (colRMSE), respectively.~~

197 To investigate the influence degrees of each physical process on ST ~~and SLW~~, we  
 198 firstly calculated the mean RMSE ( $\bar{Y}_j^i$ ) of the  $j$ th parameterization schemes ( $j = 1, 2, \dots$ )  
 199 in the  $i$ th process ( $i = 1, 2, \dots$ ). Then, the maximum difference of  $\bar{Y}_j^i$  ( $\Delta\overline{RMSE}$ ) was  
 200 defined to quantify the sensitivity of the  $i$ th process ( $i = 1, 2, \dots$ ) (Li et al., 2015):

$$201 \quad \Delta\overline{RMSE} = \bar{Y}_{max}^i - \bar{Y}_{min}^i$$

202 where  $\bar{Y}_{max}^i$  and  $\bar{Y}_{min}^i$  are the largest and the smallest  $\bar{Y}_j^i$  in the  $i$ th process,  
 203 respectively. For a given physical process, a high  $\Delta\overline{RMSE}_\tau$  signifies large difference  
 204 between parameterizations, indicating high sensitiveness of the  $i$ th process.

205 The sensitivities of physical processes were determined by quantifying the  
 206 statistical distinction level of performance between parameterization schemes. The  
 207 Independent-sample T-test (2-tailed) was adopted to identify whether the distinction  
 208 level between two schemes is significant, and that between three or more schemes was  
 209 tested using the Tukey's test. Tukey's test has been widely used for its simple  
 210 computation and statistical features (Benjamini, 2010). The detailed descriptions about  
 211 this method can be found in Zhang et al. (2016), Gan et al. (2019), and You et al. (2020).  
 212 A process can be considered sensitive when the schemes show significant difference.



213 Moreover, schemes with small mean RMSE were considered favorable for ST/SLW  
214 simulation. We distinguished the differences of the parameterization schemes at 95%  
215 confidence level.

## 216 **2.4 Optimal selection methods**

217 To extract the optimal combinations of parameterization schemes, the connection  
218 frequency (CF) between parameterizations was calculated:

- 219 (1) Sorting the 6912 colRMSEs in an ascending order;
- 220 (2) Donating the colRMSEs concentrated below the 5th percentile as the "best  
221 combinations" (346 members);
- 222 (3) Counting the times of a given parameterizations occurring with other  
223 parameterizations in the "best combinations";
- 224 (4) The CF was then determined by dividing 346.

225 Obviously, for two given parameterization schemes, a large CF has an advantage  
226 in terms of optimal combination.

## 227 **3 Results**

### 228 **3.1 General performance of the ensemble simulation**

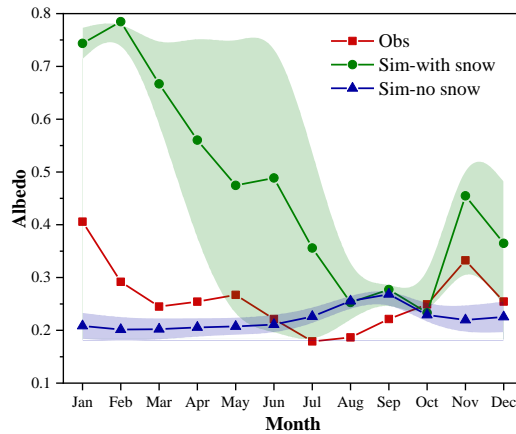
#### 229 **3.1.1 Snow process simulation**

230 The performance of Noah-MP for snow simulation and its impacts on soil  
231 temperature was firstly tested by conducting an ensemble of 41472 (= 6912\*2\*3)  
232 experiments. Due to a lack of snow depth measurements, ground albedo was used as an  
233 indicator for snow cover. Figure 1 shows the monthly variations of observed ground  
234 albedo and the simulations produced by the ensemble simulations considering snow-  
235 related physical processes (i.e. the ALB and SNF processes). The ground albedo was  
236 extremely overpredicted with large uncertainties when considering the snow options in  
237 Noah-MP, indicating the overestimation of snow depth and duration. As a result, the

238 soil temperature basically presented a huge cold bias and large uncertainties at all layers  
239 (Fig. S1). When neglecting the snow, the simulated ground albedo was nearer to the  
240 observation with a mean absolute error of 0.06. And the underestimation and  
241 uncertainties of soil temperature was greatly resolved.

242 The influence of snow cover on soil temperature was further analyzed based on in-  
243 situ measurements. Figure 3 shows the meteorological conditions and soil temperatures  
244 during a long-term snow process from 12/28/2010 – 1/27/2011. It can be seen that  
245 shallow soil temperature (5cm, 25cm, and 70cm) basically fluctuated with air  
246 temperature. At the beginning of the snow events on 1/1/2011, soil temperature at 5cm,  
247 25cm, and 70cm was slightly increased by 1.5°C, 1.2°C, and 0.7 °C, respectively. With  
248 the melting of snow, the amplitude of soil temperature decreased. Meanwhile, soil  
249 temperature at deep layers showed no obvious fluctuations during the whole period. It  
250 indicates that snow cover at TGL site has a very limited effect on soil temperature,  
251 especially that of deep layers.

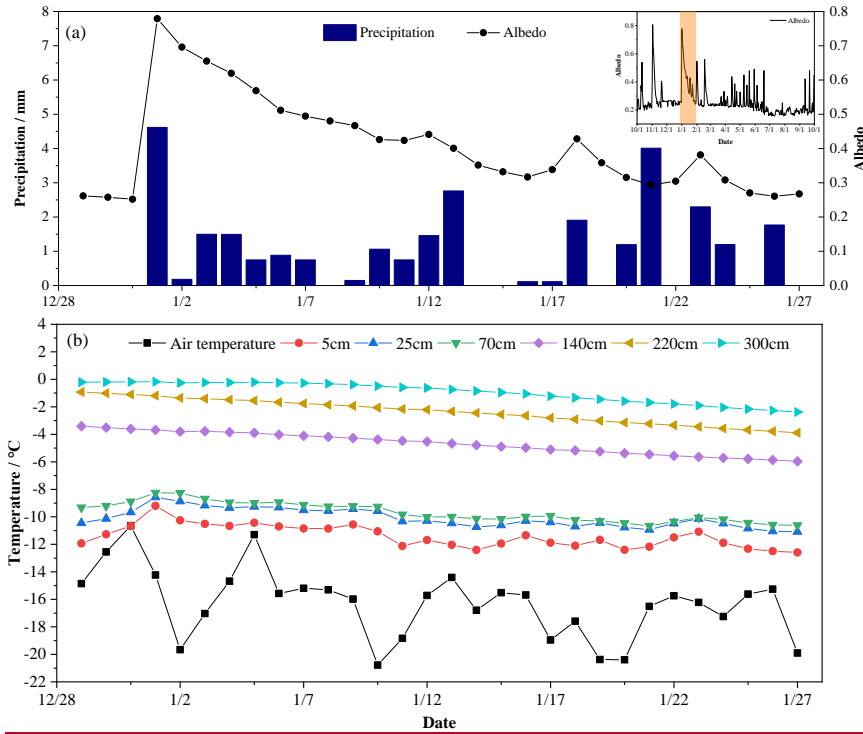
252 Given the poor simulation of Noah-MP for snow cover and the weak impact of  
253 snow on soil temperature in reality, we will focus on the results of ensemble simulations  
254 without considering snowfall (6912 experiments in total) in the following sections.



255 **Figure 2.** Monthly variations ground albedo at TGL site for observation (Obs), the  
256 ensemble simulation considering snow (Sim-with snow), and ensemble simulation  
257 neglecting snow (Sim-no snow). The green shadow represents the standard deviation  
258

259 of the ensemble simulation.

260



261

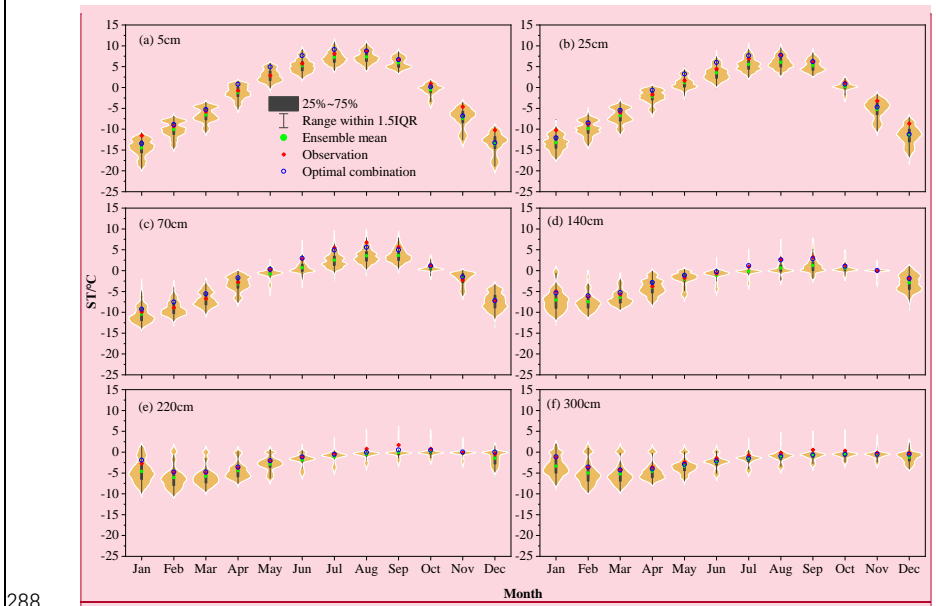
262 **Figure 3.** Variations of (a) precipitation and ground albedo, (b) air temperature and soil  
263 temperature at TGL site from 28 December 2010 to 27 January 2011.

264 **3.1.2 Soil temperature and moisture simulation**

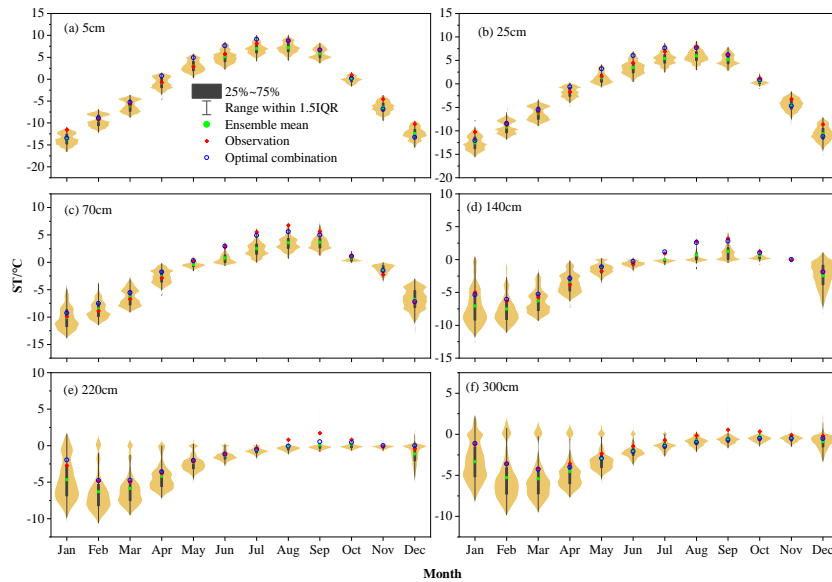
265 We evaluated ST from the 6912 experiments against observations. Figure. 2-4  
266 illustrates the ensemble simulated and observed annual cycle of ST at TGL site. The  
267 plots give the uncertainty ranges of the ensemble experiments using five statistical  
268 indicators, i.e., the first/third quartile (Q1/Q3), mean, the lower (Q1-1.5(Q3-Q1)) and  
269 upper bound (Q3+1.5(Q3-Q1)). The kernel density distribution of the simulated ST is  
270 also illustrated. The ensemble experiments basically captured the seasonal variability  
271 of ST, whose magnitude decreased with soil depth. In addition, the simulated ST in the  
272 cold season (October-April) showed relatively wide uncertainty ranges, particularly at  
273 the deep layers. This indicates that the selected schemes perform more differently

274 during the cold season, which is especially so at the deep layers. The simulated ST were  
275 generally smaller than the observations with relatively large gap during the cold season.  
276 It indicates that the Noah-MP model generally underestimates the ST, especially during  
277 the cold season. Moreover, the simulated ST was widely found to be bimodal  
278 distribution across the soil column, implying that two schemes dominate the ST  
279 simulation in the Noah-MP model.

280 Since the observation equipment can only record the liquid water, soil liquid water  
281 (SLW) was evaluated against simulations from the 6912 experiments (Fig. 5). The  
282 Noah-MP model generally underestimated surface (5cm and 25cm) and deep (300cm)  
283 SLW (Fig. 5g, 5h, 5l). However, Noah-MP tended to overestimate the SLW at the  
284 middle layers of 70cm, 140cm and 220cm. Moreover, the simulated SLW exhibited  
285 relatively wide uncertainty ranges during the warm season, particularly at the middle  
286 layers (Fig. 5). In addition, the distribution of the simulated SLW showed distinct  
287 bimodal peaks at the depth of 70cm and 140cm.

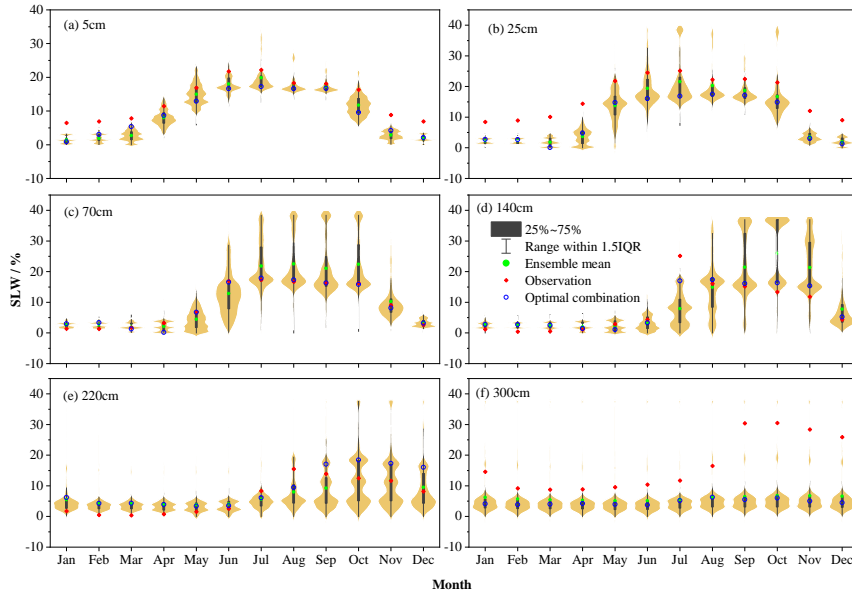


批注 [LX1]: deleted



289

290 **Figure 24.** Monthly soil temperature (ST) at (a) 5 cm, (b) 25 cm, (c) 70 cm,  
 291 (e) 220 cm, (f) 300 cm at TGL site. Limits of the boxes represent upper and lower  
 292 quartiles, whiskers extend to 1.5 times the interquartile range (IQR). The green circles  
 293 in the box are the ensemble mean values. The light orange shading represents the kernel  
 294 density distribution of simulated ST. The red diamonds are observations and the blue  
 295 circles are the results of the optimal scheme combination.



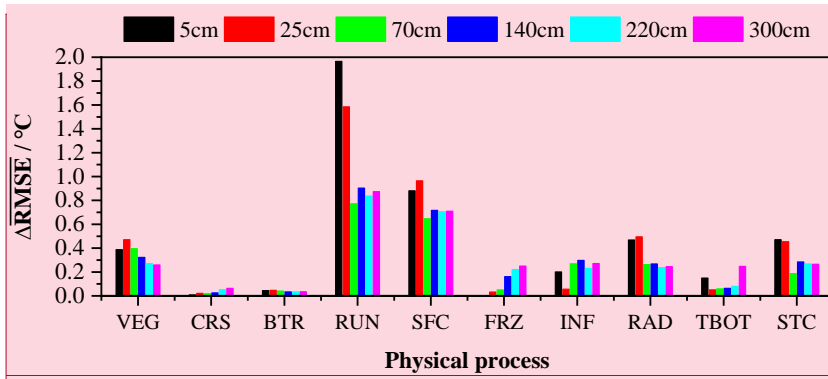
296

297

Figure 5. Same as in Figure 4 but for SLW.

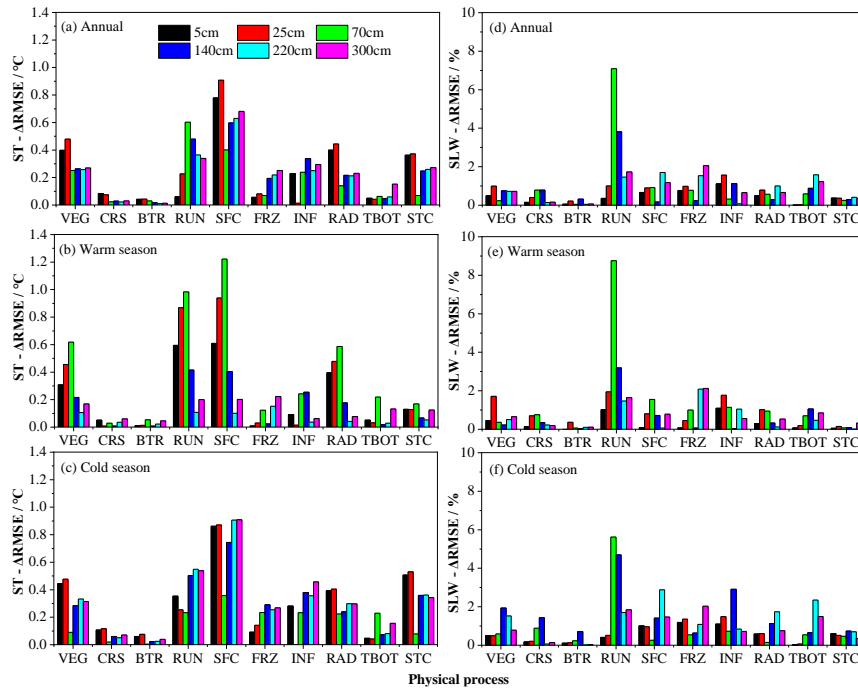
### 298 3.2 Sensitivity of physical processes

#### 299 3.2.1 Influence degrees of physical processes



300

批注 [LX2]: deleted



301

302 **Figure 36.** The maximum difference of the mean RMSE ( $\overline{\Delta ARMSE}$ ) for (a, b and c) soil  
 303 temperature ( $ST-\overline{\Delta RMSE}$  in °C) and (d, e and f) soil liquid water ( $SLW-\overline{\Delta RMSE}$  in %)  
 304 in each physical process during the (a and d) annual, (b and e) warm season, and (c and  
 305 f) cold season at different soil depths.

306 Figure. 3-6 compares the influence scores of the 10 physical processes at different  
 307 soil depths, based on the maximum difference of the mean RMSE over 6912  
 308 experiments using the same scheme, for ST and SLW at TGL site. The SFC and RUN  
 309 and SFC processes dominated the  $ST-\overline{\Delta RMSE}$  at all layers, indicating that they are the  
 310 most sensitive processes for ST simulation. While most of the  $ST-\overline{\Delta RMSE}$  of the other  
 311 8 physical processes were all less than 0.56°C, among which the influence of CRS and  
 312 BTR processes were negligible. What's more, the VEG, RAD and STC processes were  
 313 more influential on the shallow STs than the deep STs. Taking the STC-RAD process  
 314 as an example, the annual  $ST-\overline{\Delta RMSE}$  of the 5cm and 25 cm were nearly 0.54°C while  
 315 that of the 70 cm, 140cm, 220cm and 300cm were no more than around 0.32°C. In  
 316 contrast, the influence of FRZ, INF and TBOT processes were generally greater in deep

317 soils than shallow soils. During the warm season, the physical processes generally  
318 showed more influence on shallow soil temperatures. When it comes to the cold season,  
319 the influence of the physical processes on deep layers obviously increased and  
320 comparable with that on shallow layers, implying the relatively higher uncertainties of  
321 Noah-MP during the cold season.

322 Most  $\overline{\Delta RMSE}$  for SLW are far less than 10%, indicating that all the physical  
323 processes have limited influence on the SLW, among which CRS, BTR, and STC  
324 showed the smallest effects on SLW (Fig. 6d). The RUN process dominates the  
325 performance of SLW simulation, especially at lower layers (70cm and 140cm, Fig. 6d,  
326 5e, and 5f). In addition, the VEG, SFC, FRZ, RAD, and TBOT processes generally  
327 showed more influence on deep layers, particularly in the cold season.

328 Interactions between two of the most influential physical processes are analyzed  
329 in this section. The performance of the simulations with SFC and RUN were rated by  
330 rounding the colRMSEs and colSDs (Fig. 4). Given the colRMSE=1.2 for one  
331 simulation, then the score of the simulation equals 1 (SCORE=1) for the corresponding  
332 combination. It can be seen that SFC(1) in the SFC process and RUN(3) in the RUN  
333 process were the major schemes that contribute to the cold bias of the ensemble  
334 simulation, because they dominated the cold bias of the ensemble simulation with  
335 relatively low colSD scores (Fig. 4b). Consistent with the bimodal distribution in Fig.  
336 2, most of the simulations with relative low colRMSE and nearly zero colSD were  
337 related to SFC(2). It indicates that combinations with SFC(2) result in better  
338 performance than SFC(1) by improving the underestimations of ST. Among the  
339 schemes in RUN, RUN(1), RUN(2) and RUN(4) had approximately equal chance to  
340 produce better and worse performance for ST simulation, implying a dominating role  
341 of the SFC process (Fig. 4a). RUN(3) produced much worse performance by  
342 aggravating the underestimation of ST. Ultimately, the best results came from the  
343 combination of SFC(2) and RUN(4), while the worst results were from the combination  
344 of SFC(1) and RUN(3).



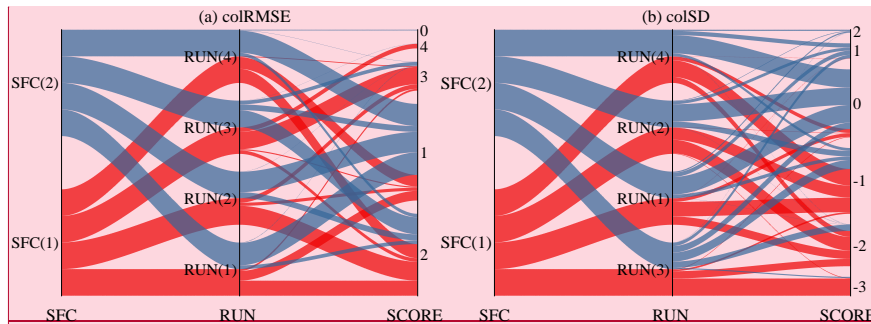


Figure 4. Rating of combinations with SFC and RUN.

批注 [LX3]: deleted

345  
346

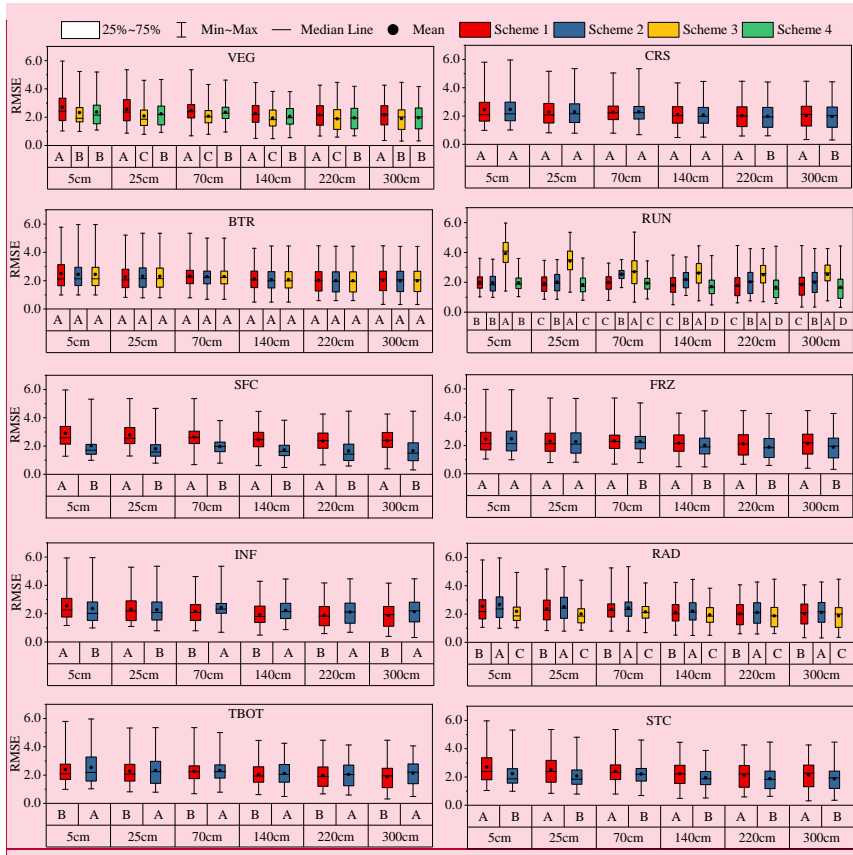
### 3.2.2 Sensitivities of physical processes and general behaviors of parameterizations

To further investigate the sensitivity of each process and the general performance of the parameterizations, the Independent-sample T-test (2-tailed) and Tukey's test were conducted to test whether the difference between parameterizations within a physical process is significant (Fig. 57). In a given sub-process, any two schemes labelled with different letters behave significantly different, and this sub-process therefore can be identified as sensitive. Otherwise, the sub-process is considered insensitive. Moreover, schemes with the letters late in the alphabet have smaller mean RMSEs and outperform the ones with the letters forward in the alphabet. Using the three schemes in vegetation model process (hereafter VEG(1), VEG(3) and VEG(4)) in Fig. 5-7 as an example. At the depth of ~~5cm-70cm and 300cm~~, VEG(~~13~~) was labeled with letter "~~A~~B", while VEG(~~31~~) and VEG(4) was labeled with letter "~~B~~A". For ~~other layers, the depth of 25cm, 70cm, 140cm and 220cm~~, VEG(1), VEG(3) and VEG(4) were labeled with the letter "A", "C" and "B", respectively. As described above, the VEG process was sensitive for ST simulation. Moreover, VEG(3) ~~and VEG(4)~~ had advantages in producing good simulations than VEG(1) ~~and VEG(4)~~ at ~~5cm-70cm and 300cm~~ depths, and the performance decreased in the order of VEG(3) > VEG(4) > VEG(1) at other layers. In terms of the whole soil column, VEG(3) outperformed VEG(1) and VEG(4).

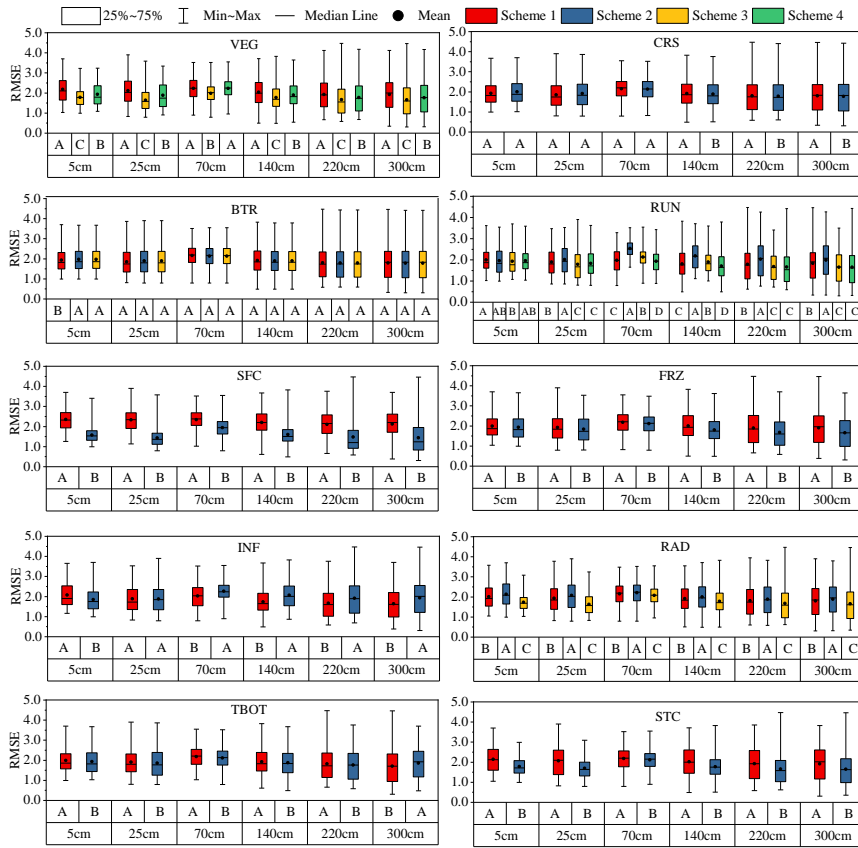
Consistent with the result in Fig. 36, all other physical processes showed sensitivities in varying magnitudes except the BTR and CRS process. And the

366  
367

368 performance difference between schemes of the RUN and SFC were obviously greater  
369 than other processes. For the RUN process, the performance orders for both ST and  
370 SLW simulation generally followed RUN(4) > RUN(1) > RUN(2) > RUN(3) as a  
371 whole. For the whole year, RUN(1), RUN(3), and RUN(4) had significant but slightly  
372 difference between each other, among which RUN(1) and RUN(4) presented similar  
373 performance during both warm and cold seasons (Fig. S2, S3, S4 and S5). During the  
374 warm season, the performance of RUN(3) for ST simulation showed notable  
375 improvements at shallow layers (5cm and 25cm, Fig. S2). By contrast, RUN(2)  
376 performed the worst among the four schemes in spite of the good performance at  
377 shallow layers during the cold season (5cm and 25cm in Fig. S3, 25cm in Fig. S5).  
378 Meanwhile, the difference between RUN(1) and RUN(4) was indistinctive at the  
379 shallow layers (5 cm, 25 cm and 70 cm) and significant but very small at the deep layers  
380 (140 cm, 220 cm and 300 cm). During both warm and cold seasons, Moreover, the  
381 performance orders for ST simulations were SFC(2) > SFC(1) for SFC process, FRZ(2) >  
382 FRZ(1) for FRZ process, and RAD(3) > RAD(1) > RAD(2) for RAD process (Fig. S2  
383 and S3), TBOT(1) > TBOT(2) for TBOT process, and STC(2) > STC(1) for STC  
384 process which are particularly so for SLW simulations at shallow and deep layers. In  
385 particular, the FRZ process showed higher sensitivity at the deep soils and during the  
386 cold season (Fig. 6, 7 and 8). in spite of the shallow soil. For the ST simulation,  
387 Compared with INF(1), INF(2) performed better at the shallow soils (5cm and 25cm)  
388 while did worse at the deep soils compared with INF(1). Despite the slightly good  
389 performance of TBOT(2) for ST simulation at the first five layers, TBOT(1) greatly  
390 outperformed TBOT(2) at the depth of 300cm. For the STC process, STC(2) greatly  
391 excel STC(1) in simulating ST while showed small different with STC(1) when  
392 simulating SLW. However, the impact of STC process on SLW increase in line with  
393 that on ST during the cold season (Fig. 6).



批注 [LX4]: deleted



395

396 **Figure 57.** Distinction level for RMSE of ST at different layers during the whole year  
 397 in the ensemble simulations. Limits of the boxes represent upper and lower quartiles,  
 398 whiskers extend to the maximum and minimum RMSE. The black stations in the box  
 399 are the average values. The lines in the box indicate the median value.

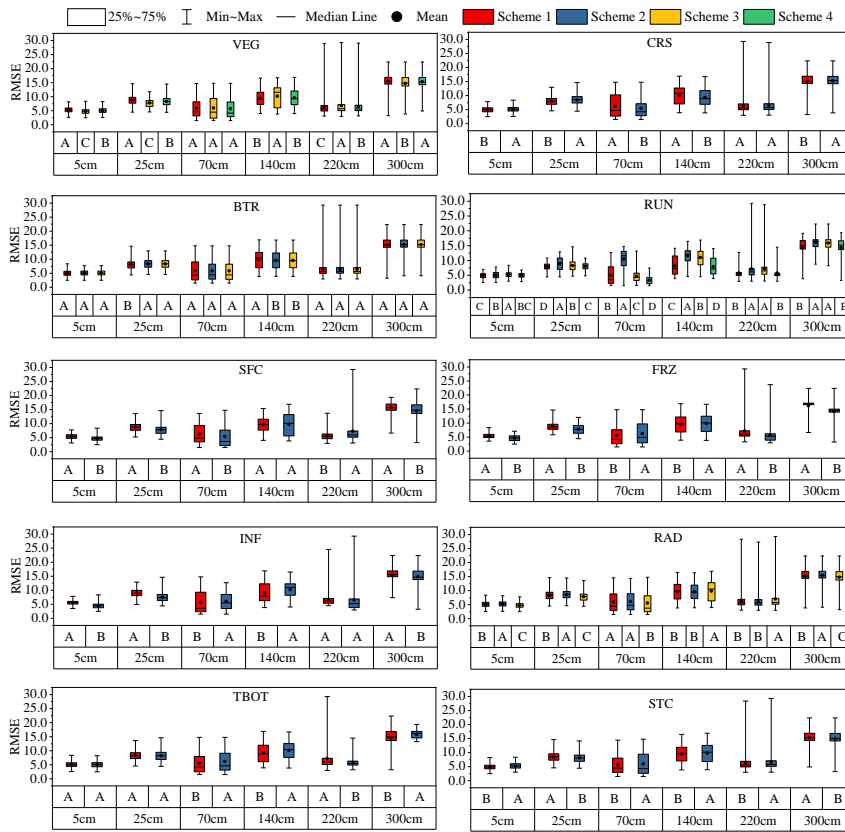


Figure 8. Same as in Figure 7 but for SLW.

### 3.3 The optimal combination

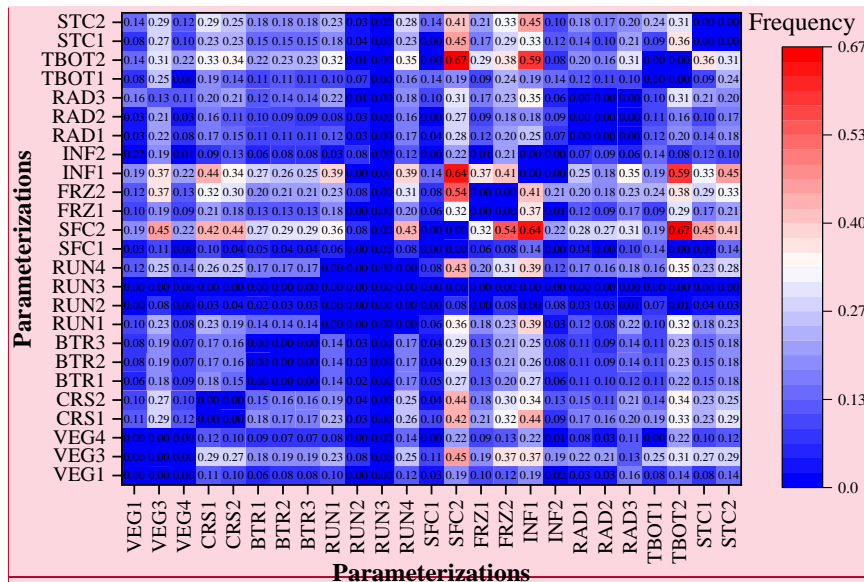
The CF was calculated to extract the optimal combination of parameterization schemes for ST simulation (Fig. 69). The CF between any two schemes from the same physical process was zero as expected. Consistent with Fig. 5, the CF of RUN(2) and RUN(3) with other schemes was nearly zero, implying that using RUN(2) and RUN(3) provides an extreme less chance of producing favorable simulations than using RUN(1); RUN(2) or RUN(4). A higher CF signify greater probability of producing advantageous simulations. For instance, the CF between SFC(2) and VEG(3) was 0.4546, about two times than the CFs between SFC(2) and VEG(1)/VEG(4). It indicates that 4546% of the 346 best combinations adopted SFC(2) and VEG(3) simultaneously, and the

412 combination of SFC(2) and VEG(3) tend to ~~indueing~~induce better ST in comparison  
413 of the combination of SFC(2) and VEG(1)/VEG(4).

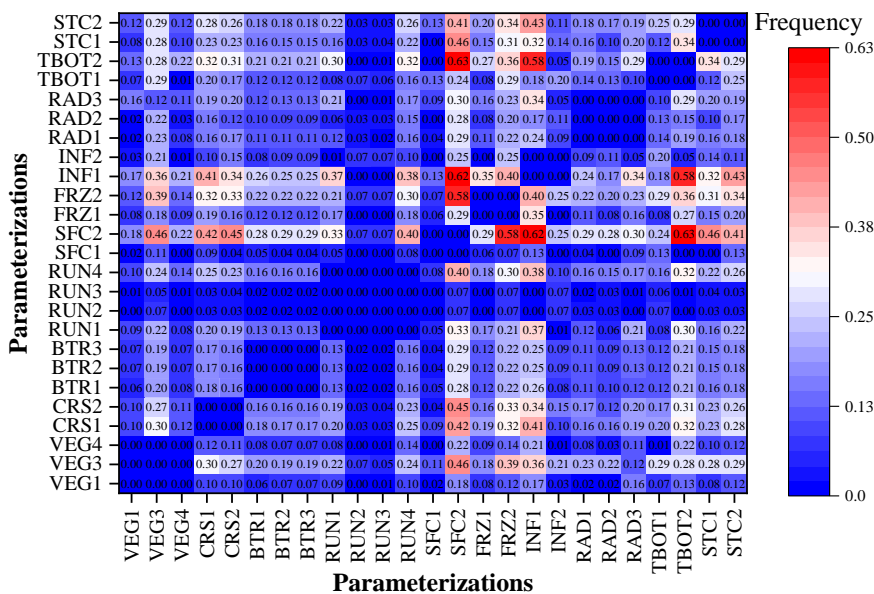
414 SFC(2) is firstly determined as one of the schemes that make up the optimal  
415 combination, because it was most widely linked to other parameterization schemes with  
416 relatively large CFs. Other optimal schemes of each physical process can be determined  
417 by choosing the one that has large CF with SFC(2). Obviously, VEG(3), RUN(4),  
418 FRZ(2) and INF(1) outperform other schemes in the corresponding physical processes  
419 and were selected for optimal combination. The schemes within CRS, BTR, RAD and  
420 STC processes scored nearly identical CFs with SFC(2). Due to the insensitivity of CRS  
421 and BTR, CRS(1) and BTR(1), which are the default schemes in Noah-MP, were  
422 determined as the member schemes of the optimal combination. Combining the selected  
423 schemes above with different schemes of RAD and STC processes, there are 6  
424 candidate combinations, among which the one with smallest colRMSE is selected as  
425 the optimal combination. Ultimately, the determined schemes for optimal combination  
426 is VEG(3), CRS(1), BTR(1), RUN(4), SFC(2), FRZ(2), INF(1), RAD(2), TBOT(2) and  
427 STC(1) (Table 1).

428 The simulated results of the optimal scheme combination well captured the  
429 variation of ST (Fig. 24). Despite the overestimation of ST at the shallow soil layers  
430 from April to July, the optimal combination well produced the ST during the cold season  
431 and of the deep layers (Fig. 24), which is crucial for modeling permafrost features such  
432 as active layer thickness and temperature at the top of the permafrost.

433



434



435

436

Figure 69. Connection frequency of parameterization schemes.

## 437 4 Discussion

### 438 4.1 Influence of snow cover on permafrost in the QTP

439 Reproducing the snow processes remains a persistent challenge for LSMs in the  
440 QTP, most of which overestimate the snow depth (Wei and Dong, 2015), including the  
441 Noah-MP model (Jiang et al., 2020; Li et al., 2020; Wang et al., 2020). Our ensemble  
442 simulations also show that the surface albedo is extremely overestimated in both  
443 magnitude and duration (Fig. 2), implying an extreme overestimation of snow cover.  
444 The overestimation is ascribed to many causes, such as the vegetation effect (Park et  
445 al., 2016), the snow cover fraction (Jiang et al., 2020), the sublimation from wind (Yuan  
446 et al., 2016; Li et al., 2020), and the fresh snow albedo (Wang et al. 2020). More need  
447 to be done in the future to quantify the influence of these physics.

448 However, snow cover in the permafrost regions of the QTP is thin, patchy, and  
449 short-lived (Che et al., 2019) because of the high wind speed (Yuan et al., 2016; Xie et  
450 al., 2019) and strong solar radiation (Meng et al., 2018). Its influence on soil  
451 temperature and contribution to permafrost state is usually considered weak (Jin et al.,  
452 2008). The in-situ measurements at TGL site also showed limited influence on soil  
453 temperature (Fig. 3), which is consistent with the studies at an alpine wetland site  
454 (Zhang et al., 2018) and the Yellow River source (Yao et al., 2019) on the QTP. The  
455 insufficient of numerical models for snow simulation seriously suppresses the accuracy  
456 of soil temperature (Fig. S1). For practical purpose, the snow processes is usually  
457 neglected when modeling the permafrost state in the QTP (Qin et al., 2017; Zou et al.,  
458 2017; Wu et al., 2018).

#### 459 4.1.2 Possible reasons for the cold bias of soil temperature

460 The cold bias of soil temperature on the QTP are widely reported in many of the  
461 state-of-the-art LSMs (Yang et al., 2009; Chen et al., 2019). One of the main reason can  
462 be the inability of representing the diurnal variation of roughness length for heat ( $Z_{0h}$ )



463 on the QTP ( Yang et al., 2008; Chen et al., 2010), which is of great importance for a  
464 reliable calculation of the sensible and latent heat, and thus for the soil surface/profile  
465 temperature calculation (Zeng et al., 2012; Zheng et al., 2012). Noah-MP parameterize  
466  $Z_{0h}$  in the two schemes of SFC process (Table 1). In the M-O scheme,  $Z_{0h}$  is taken as  
467 the same with the roughness length for momentum ( $Z_{0m}$ , Niu et al., 2011). The Chen97  
468 scheme adopts the Zilitinkevitch approach (Zilitinkevich, 1995). However, both of  
469 them couldn't produce the diurnal variation of  $Z_{0,h}$  (Chen et al., 2010).

470 Another possible reason is the poor representation of the thermal conductivity ( $\lambda$ )  
471 of frozen soil. Considering that the  $\lambda$  of ice is nearly four times higher than liquid  
472 water,  $\lambda$  of frozen soil is generally expected to be greater than that of unfrozen soil.  
473 Many parameterization schemes of  $\lambda$ , including the Johansen scheme in Noah-MP,  
474 follow this pattern (Du et al., 2020). However, contrary phenomenon is widely reported  
475 over the QTP (Pan et al., 2016; Hu et al., 2017; Yi et al., 2018; Li et al., 2019), including  
476 the TGL site (Li et al., 2019). As a result, a majority of the state-of-the-art LSMs have  
477 tended to overestimate the soil thermal conductivity of the QTP (Luo et al., 2009; Chen  
478 et al., 2012; Du et al., 2020), which exactly explains the underestimation of soil  
479 temperature during cold season and, at times, an overestimation during the warm season  
480 (Luo et al., 2009).

#### 481 4.24.3 Discussions on the sensitivity of physical processes

##### 482 **4.23.1 Vegetation model (VEG) and canopy gap for radiation transfer (RAD)**

483 Noah-MP computes energy fluxes in vegetated fraction and bare fraction  
484 separately and then sum them up weighted by vegetation fraction (FVEG). As list in  
485 Table 1, VEG process includes three options to calculate the variation of ~~vegetation~~  
486 ~~fraction (FVEG)-FVEG~~ in this study. VEG(3) calculates the daily FVEG based on the  
487 interpolated LAI, while VEG(1) and VEG(4) uses the prescribed monthly and  
488 maximum LAI FVEG, respectively. Obviously, VEG(3) produces more realistic FVEG  
489 over the year, followed by VEG(1) and VEG(4). VEG(4) grossly overestimates the  
490 FVEG, especially that during the cold season. Consequently, VEG(3) outperformed

491 VEG(1) and VEG(4). However, VEG(4) is widely used in many studies (Gao et al.,  
492 2015; Chen et al., 2016; Li et al., 2018) despite overestimating the FVEG. In this study,  
493 VEG(4) performed better than VEG(1).

494 RAD treats the radiation transfer process within the vegetation, and adopts three  
495 methods to calculate the canopy gap. RAD(1) defines canopy gap as a function of the  
496 3D vegetation structure and the solar zenith angle, RAD(2) employs no gap within  
497 canopy, and RAD(3) treat the canopy gap from unity minus the FVEG (Niu and Yang,  
498 2004). The RAD(3) scheme penetrates the most solar radiation to the ground, followed  
499 by the RAD(1) and RAD(2) schemes. As an alpine grassland, there is a relative low  
500 LAI at TGL site, and thus a quite high canopy gap. So, schemes with a larger canopy  
501 gap could realistically reflect the environment. Consequently, the performance  
502 decreased in the order of RAD(3) > RAD(1) > RAD(2) for ST/SLW simulation.

#### 503 **4.23.2 Canopy stomatal resistance (CRS) and soil moisture factor for stomatal** 504 **resistance (BTR)**

505 The biophysical process BTR and CRS directly affect the canopy stomatal  
506 resistance and thus the plant transpiration (Niu et al., 2011). The transpiration of plants  
507 could impact the ST through its cooling effect (Shen et al., 2015) and the water balance  
508 of root zone (Chang et al., 2020). However, the annual transpiration of alpine steppe is  
509 weak due to the shallow effective root zone and lower stomatal control in this dry  
510 environment (Ma et al., 2015), ~~which may explain the indistinctive or very small~~  
511 ~~difference among the schemes of the BTR and CRS processes (Fig. 7 and 8). As a result,~~  
512 ~~the BTR process was insensitive at all layers. CRS(1) and CRS(2) had no significant~~  
513 ~~difference at most layers except the last two layers. However, the performance~~  
514 ~~difference between CRS(1) and CRS(2) at the last two layers is very small (Fig. 3 and~~  
515 ~~5).~~

#### 516 **4.23.3 Runoff and groundwater (RUN)**

517 For the RUN process, RUN(32) had the worst performance for simulating ~~soil~~  
518 ~~moisture (Fig. S1) and thus for ST and SLW (Fig. 57 and 8) among the four schemes,~~

519 likely due to its higher estimation of soil moisture (Fig. S6) and thus greater sensible  
520 heat and smaller ST (Gao et al., 2015). free drainage assumption for subsurface runoff  
521 (Schaake et al., 1996), which is partly consistent with the study of Zhang et al. (2016)  
522 that RUN(3) is the worst performing scheme for sensible and latent heat simulation in  
523 most cases compared with RUN(1) and RUN(2). RUN(4) also adopts the free drainage  
524 concept. Consistent with the study of Li et al. (2015), RUN(3) performed the best at  
525 shallow layers for ST during the warm season, while that for SLW were less good.  
526 However, RUN(4) outperformed RUN(3) at deep layers, which may be explained by  
527 the better agreement of SLW by RUN(4) (Fig. 8 and S6). It can be explained by the  
528 fourth power function of wetness at the top 2-m soil in RUN(4), in which the partition  
529 of surface runoff and infiltration is regulated by soil moisture (Yang and Dickinson,  
530 1996). Likewise, RUN(4) was on a par with RUN(1) in the simulation of ST due to the  
531 very small difference in SLW of two schemes (Fig. 8 and S6). unfrozen water (Fig. S1).  
532 Consequently, there was no or very small difference between RUN(4) and RUN(1) at  
533 shallow/deep soils (Fig. 5). For the whole soil column, RUN(4) surpassed RUN(1) and  
534 RUN(2), both of which define surface/subsurface runoff as functions of groundwater  
535 table depth (Niu et al., 2005; Niu et al., 2007). This is in keeping with the study of  
536 Zheng et al. (2017) that soil water storage-based parameterizations outperform the  
537 groundwater table-based parameterizations in simulating the total runoff in a seasonally  
538 frozen and high-altitude Tibetan river, Besides, RUN(4) is designed based on the  
539 infiltration-excess runoff (Yang and Dickinson, 1996) in spite of the saturation-excess  
540 runoff in RUN(1) and RUN(2) (Gan et al., 2019), which is more common in arid and  
541 semiarid areas like the permafrost regions of QTP (Pilgrim et al., 1988).

#### 542 **4.2.3.4 Surface layer drag coefficient (SFC)**

543 SFC defines the calculations of the surface exchange coefficient for heat and water  
544 vapor (CH), which greatly impact the energy and water balance and thus the  
545 temperature and moisture of land surfacesoil. SFC(1) adopts the Monin-Obukhov  
546 similarity theory (MOST) with a general form, while the SFC(2) uses the improved  
547 MOST modified by Chen et al. (1997). The most distinct difference between them is

548 that SFC(1) considers the zero-displacement height while SFC(2) parameterizes  $Z_{0h}$  and  
549  $Z_{0m}$  using different schemes. The difference between SFC(1) and SFC(2) has a great  
550 impact on the CH value. Several studies have reported that SFC(2) has a better  
551 performance for the simulation of sensible and latent heat on the QTP (Zhang et al.,  
552 2016; Gan et al., 2019). The results of Tukey's-T-test in this study showed remarkable  
553 distinctions between the two schemes, where SFC(2) was dramatically superior to  
554 SFC(1) (Fig. S7 and 8). SFC(2) produces lower CH than SFC(1) (Zhang et al., 2014),  
555 resulting in less efficient ventilation and greater heating of the land surface (Yang et al.,  
556 2011b), and substantial improvement of the cold bias of Noah-MP in this study (Fig. 4).  
557 As the sensible heat rising, the latent heat decline (Gao et al., 2015) and the dry bias of  
558 Noah-MP is mitigated (Fig. 8).

#### 559 **4.23.5 Super-cooled liquid water (FRZ) and frozen soil permeability (INF)**

560 FRZ treats ~~unfrozen water~~liquid water (super-cooled liquid water) in frozen soil  
561 (super-cooled liquid water) using two forms of freezing-point depression equation.  
562 FRZ(1) takes a general form (Niu and Yang, 2006), while FRZ(2) exhibits a variant  
563 form that considers the increased surface area of icy soil particles (Koren et al., 1999).  
564 FRZ(2) generally yields more liquid water in comparison of FRZ(1). In this studyFor  
565 ST simulation, FRZ process did not show sensitivity at the shallow soil layers (5cm and  
566 25cm) during the warm season (Fig. S2), but showed an increasing sensitivity at the  
567 deep layers, especially during the cold season (Fig. 34 and S3), ~~which~~This can be  
568 related to the greater sensitivity of FRZ (Fig. 4, S4 and S5) and the longer frozen  
569 duration ~~of at~~ at deep soil and during the cold season.

570 INF(1) uses soil moisture (Niu and Yang, 2006) while INF(2) employs only the  
571 liquid water (Koren et al., 1999) to parameterize soil hydraulic properties. INF(2)  
572 generally produces more impermeable frozen soil than INF(1), which is also found in  
573 this study (Fig. S2S7). Due to the more realistic representation of ~~unfrozen water~~SLW  
574 during the cold season (Fig. S2S7), INF(2) surpassed INF(1) in simulating ST at 5 cm  
575 ~~and 25 cm~~ depth, while INF(1) outperformed INF(2) at 70 cm, 140 cm and 220 cm (Fig.  
576 S7). This result also indicate that INF(1) and INF(2) could alleviate the overestimation

577 and underestimation of ~~unfrozen water~~SLW, respectively. INF(2) ~~performed simulated~~  
578 worse ST than INF(1) at 300 cm depth (Fig. 57) in spite of the better agreement with  
579 ~~unfrozen water~~observed SLW (Fig. S28 and S7), which may be related to the  
580 overestimation of soil moisture of INF(2) at the depth of 140 cm.

#### 581 **4.23.6 Lower boundary of soil temperature (TBOT) and snow/soil temperature** 582 **time scheme (STC)**

583 TBOT process adopts two schemes to describe the soil temperature boundary  
584 conditions. TBOT (1) assumes zero heat flux at the bottom of the model, while TBOT(2)  
585 adopts the soil temperature at the 8 m depth (Yang et al., 2011a). In general, TBOT(1)  
586 is expected to accumulate heat in the deep soil and produce higher ST than TBOT(2).  
587 In this study, the two assumptions performed significantly different, especially at the  
588 deep soil. Although TBOT(2) is more representative of the realistic condition, TBOT(1)  
589 greatly surpassed TBOT(2) at the depth of 300cm in this study. It can be related to the  
590 overall underestimation of the model, which can be alleviated by TBOT(1) because of  
591 heat accumulation (Fig. S3S8).

592 Two time discretization strategies are implemented in the STC process, where  
593 STC(1) adopts the semi-implicit scheme while STC(2) uses the full implicit scheme, to  
594 solve the thermal diffusion equation in first soil or snow layers (Yang et al., 2011a).  
595 STC(1) and STC(2) are not strictly a physical processes but different upper boundary  
596 conditions of soil column (You et al., 2019). The differences between STC(1) and  
597 STC(2) were significant (Fig. 57). Snow processes are not involved in this study, the  
598 impacts of the two options on ST is remarkable (Fig. 56), particularly in the shallow  
599 layers and during the cold season (Fig. 36). In addition, STC(2) outperformed STC(1)  
600 in the ensemble simulation experiments simulated ST (Fig. 57), because the higher ST  
601 produced by STC(2) (Fig. S4S9) alleviated the overall underestimation of Noah-MP.

#### 602 **4.34.4 Perspectives**

603 This study analyzed the characteristics and general behaviors of each

604 parameterization scheme of Noah-MP at a typical permafrost site on the QTP, hoping  
605 to provide a reference for simulating permafrost state on the QTP. We identified the  
606 systematic overestimation of snow cover and cold bias in Noah-MP, and discussed the  
607 possible sources of error. Relevant results and methodologies can be practical  
608 guidelines for improving the parameterizations of physical processes and testing their  
609 uncertainties towards near-surface permafrost modeling on the plateau. Although the  
610 site we selected may be representative for the typical environment on the plateau,  
611 continued investigation with a broad spectrum of climate and environmental conditions  
612 is required to make a general conclusion at regional scale.

613 ~~We identified the systematic cold bias of Noah-MP and discussed the possible~~  
614 ~~sources of error, and analyzed the characteristics and general behavior of each~~  
615 ~~parameterization scheme at a permafrost site on the QTP. This work would be~~  
616 ~~constructive to a better understanding of the land surface processes on the QTP and~~  
617 ~~further model improvements towards near-surface permafrost modeling using the~~  
618 ~~LSMs.~~

619 ~~Although the optimal combination demonstrated in this study is only from the~~  
620 ~~selected site, our results provide a practical way to investigate the permafrost state on~~  
621 ~~the QTP. The optimal combination well simulated the ST, especially that of deep layers~~  
622 ~~(Fig. 2). The representation of deep ST is crucial for permafrost modeling, which~~  
623 ~~directly affects the permafrost features such as active layer thickness and temperature~~  
624 ~~at the top of the permafrost. Further investigation with a broad spectrum of climate and~~  
625 ~~environmental conditions is necessary to make a general conclusion.~~

## 626 **5 Conclusions**

627 In this study, an ensemble simulation ~~of soil temperature~~ using multi-  
628 parameterizations was conducted using the Noah-MP model at the TGL site, aiming to  
629 provide a reference for permafrost simulation using LSMs. The model was modified to  
630 consider the vertical heterogeneity in the soil and the simulation depth was extended to  
631 cover the whole active layer. The ensemble simulation consists of 6912

632 parameterization experiments, combining ten physical processes (VEG, CRS, BTR,  
633 RUN, SFC, FRZ, INF, RAD, TBOT, and STC) each with multiple optional schemes.

634 On this basis, the general performance of Noah-MP was assessed by comparing  
635 simulation results with in situ observations, and the sensitivity of soil temperature and  
636 moisture at different depth of active layer to parameterization schemes was explored.

637 Furthermore, we proposed a new method to extract the optimal combination of schemes  
638 to simulate soil temperature in the permafrost regions of the QTP. The main conclusions  
639 are as follows:

640 (1) Noah-MP model tends to overestimate snow cover and thus largely underestimate  
641 soil temperature in the permafrost regions of the QTP. Systematic cold bias and  
642 large uncertainties of soil temperature still exist after removing the snow processes,  
643 has relatively large uncertainties in the cold season, particularly at the deep layers  
644 and during the cold season. Moreover, the model tends to underestimate soil  
645 temperature, especially during the cold season. This is largely due to the imperfect  
646 model structure with regard to the roughness length for heat and soil thermal  
647 conductivity.

648 (2) Soil temperature is dominated by the surface layer drag coefficient (SFC) while  
649 largely influenced by runoff and groundwater (RUN). SFC(2) and RUN(3) could  
650 significantly alleviate and aggravate the cold bias of soil temperature, respectively.

651 Other physical processes have little impact on ST simulation, among which VEG,  
652 RAD, and STC are more influential on shallow ST, while FRZ, INF and TBOT have  
653 greater impacts on deep ST. In addition, CRS and BTR do not significantly affect  
654 the simulation results.

655 (3) The best scheme combination for permafrost simulation are as follows: VEG (table  
656 LAI, calculated vegetation fraction), CRS (Jarvis), BTR (Noah), RUN (BATS),  
657 SFC (Chen97), RAD (zero canopy gap), FRZ (variant freezing-point depression),  
658 INF (hydraulic parameters defined by soil moisture), TBOT (ST at 8 m), STC (semi-  
659 implicit).

660

661 *Code availability.* The source code of offline 1D Noah-MP LSM v1.1 is available at  
662 <https://ral.ucar.edu/solutions/products/noah-multiparameterization-land-surface->  
663 [model-noah-mp-lsm](https://ral.ucar.edu/solutions/products/noah-multiparameterization-land-surface-model-noah-mp-lsm) (last access: 15 May 2020). The modified Noah-MP with the  
664 consideration of vertical heterogeneity, extended soil depth, and pedotransfer functions  
665 is available upon request to the corresponding author. The data processing code are  
666 available at <http://dx.doi.org/10.17632/gc7vfgkyng.1>.

667

668 *Data availability.* The 1-hourly forcing data and daily soil temperature data at the TGL  
669 site are available at <http://dx.doi.org/10.17632/gc7vfgkyng.1>. Soil texture data can be  
670 obtained at <https://doi.org/10.1016/j.catena.2017.04.011> (Hu et al., 2017). The AVHRR  
671 LAI data can be downloaded from <https://www.ncei.noaa.gov/data/> (Claverie et al.,  
672 2016).

673

674 *Author contributions.* TW and XL conceived the idea and designed the model  
675 experiments. XL performed the simulations, analyzed the output, and wrote the paper.  
676 XW, XZ, GH, RL contributed to the conduction of the simulation and interpretation of  
677 the results. YQ provided the observations of atmospheric forcing and soil temperature.  
678 CY and JH helped in downloading and processing the AVHRR LAI data. JN and WM  
679 provide guidelines for the visualization. Everyone revised and polished the paper.

680

681 *Competing interests.* The authors declare that they have no conflict of interest.

682

683 *Acknowledgements.* This work has been supported by [the CAS "Light of West China"](#)  
684 [Program, and](#) the National Natural Science Foundation of China (41690142; 41771076;  
685 41961144021; 41671070). The authors ~~also~~ thank Cryosphere Research Station on the  
686 Qinghai-Tibet Plateau, CAS for providing field observation data used in this study. [We](#)  
687 [would like to thank two anonymous reviewers for their insightful and constructive](#)  
688 [comments and suggestions, which greatly improved the quality of the manuscript.](#)



689 **References**

- 690 Benjamini, Y.: Simultaneous and selective inference: Current successes and future challenges,  
691 *Biometrical J.*, 52, 708-721, <https://doi.org/10.1002/bimj.200900299>, 2010.
- 692 Cao, B., Zhang, T., Wu, Q., Sheng, Y., Zhao, L., and Zou, D.: Brief communication: Evaluation and  
693 inter-comparisons of Qinghai-Tibet Plateau permafrost maps based on a new inventory of field  
694 evidence, *The Cryosphere*, 13, 511-519, <https://doi.org/10.5194/tc-13-511-2019>, 2019.
- 695 Chang, M., Liao, W., Wang, X., Zhang, Q., Chen, W., Wu, Z., and Hu, Z.: An optimal ensemble of  
696 the Noah-MP land surface model for simulating surface heat fluxes over a typical subtropical  
697 forest in South China, *Agric. For. Meteorol.*, 281, 107815,  
698 <https://doi.org/https://doi.org/10.1016/j.agrformet.2019.107815>, 2020.
- 699 Che, T., Hao, X., Dai, L., Li, H., Huang, X., and Xiao, L.: Snow cover variation and its impacts over  
700 the Qinghai-Tibet Plateau, *Bull. Chin. Acad. Sci.*, 34, 1247-1253,  
701 <https://doi.org/10.16418/j.issn.1000-3045.2019.11.007>, 2019.
- 702 Chen, F., Janjić, Z., and Mitchell, K.: Impact of atmospheric surface-layer parameterizations in the  
703 new land-surface scheme of the NCEP Mesoscale Eta Model. *Boundary-Layer Meteorol.* 85, 391-  
704 421, <https://doi.org/10.1023/A:1000531001463>, 1997.
- 705 Chen, L., Li, Y., Chen, F., Barr, A., Barlage, M., and Wan, B.: The incorporation of an organic soil  
706 layer in the Noah-MP land surface model and its evaluation over a boreal aspen forest, *Atmos.*  
707 *Chem. Phys.*, 16, 8375-8387, <https://doi.org/10.5194/acp-16-8375-2016>, 2016.
- 708 Chen, R., Yang, M., Wang, X., and Wan, G.: Review on simulation of land-surface processes on the  
709 Tibetan Plateau, *Sci. Cold Arid Reg.*, 11, 93-115, <https://doi.org/10.3724/SP.J.1226.2019.00093>,  
710 2019.
- 711 Chen, S., Li, X., Wu, T., Xue, K., Luo, D., Wang, X., Wu, Q., Kang, S., Zhou, H., and Wei, D.: Soil  
712 thermal regime alteration under experimental warming in permafrost regions of the central  
713 Tibetan Plateau, *Geoderma*, 372, 114397,  
714 <https://doi.org/https://doi.org/10.1016/j.geoderma.2020.114397>, 2020.
- 715 Chen, Y., Yang, K., Zhou, D., Qin, J., and Guo, X.: Improving the Noah Land Surface Model in Arid  
716 Regions with an Appropriate Parameterization of the Thermal Roughness Length, *J.*  
717 *Hydrometeorol.*, 11, 995-1006, <https://doi.org/10.1175/2010JHM1185.1>, 2010.
- 718 Chen, Y., Yang, K., Tang, W., Qin, J., and Zhao, L.: Parameterizing soil organic carbon's impacts  
719 on soil porosity and thermal parameters for Eastern Tibet grasslands, *Sci. Chin. Earth Sci.*, 55,  
720 1001-1011, <https://doi.org/10.1007/s11430-012-4433-0>, 2012.
- 721 Claverie, M., Matthews, J. L., Vermote, E. F., and Justice, C. O.: A 30+ Year AVHRR LAI and  
722 FAPAR Climate Data Record: Algorithm Description and Validation, *Remote Sens.*, 8, 263,  
723 <https://doi.org/10.3390/rs8030263>, 2016.
- 724 Cosby, B. J., Hornberger, G. M., Clapp, R. B., and Ginn, T. R.: A Statistical Exploration of the  
725 Relationships of Soil Moisture Characteristics to the Physical Properties of Soils, *Water Resour.*  
726 *Res.*, 20, 682-690, <https://doi.org/10.1029/WR020i006p00682>, 1984.
- 727 Daniel, R., Nikolay, S., Bernd, E., Stephan, G., and Sergei, M.: Recent advances in permafrost  
728 modelling, *Permafrost. Periglac. Process.*, 19, 137-156, <https://doi.org/doi:10.1002/ppp.615>, 2008.
- 729 Du, Y., Li, R., Zhao, L., Yang, C., Wu, T., Hu, G., Xiao, Y., Zhu, X., Yang, S., Ni, J., and Ma, J.:  
730 Evaluation of 11 soil thermal conductivity schemes for the permafrost region of the central

731 Qinghai-Tibet Plateau, CATENA, 193, 104608,  
732 <https://doi.org/https://doi.org/10.1016/j.catena.2020.104608>, 2020.

733 Fountain, A. G., Campbell, J. L., Schuur, E. A. G., Stammerjohn, S. E., Williams, M. W., and  
734 Ducklow, H. W.: The Disappearing Cryosphere: Impacts and Ecosystem Responses to Rapid  
735 Cryosphere Loss, *BioScience*, 62, 405-415, <https://doi.org/10.1525/bio.2012.62.4.11>, 2012.

736 Gan, Y. J., Liang, X. Z., Duan, Q. Y., Chen, F., Li, J. D., and Zhang, Y.: Assessment and Reduction  
737 of the Physical Parameterization Uncertainty for Noah-MP Land Surface Model, *Water Resour.*  
738 *Res.*, 55, 5518-5538, <https://doi.org/10.1029/2019wr024814>, 2019.

739 Gao, Y., Kai, L., Fei, C., Jiang, Y., and Lu, C.: Assessing and improving Noah-MP land model  
740 simulations for the central Tibetan Plateau, *J. Geophys. Res.-Atmos.*, 120, 9258-9278, 2015.

741 Guo, D., and Wang, H.: Simulation of permafrost and seasonally frozen ground conditions on the  
742 Tibetan Plateau, 1981-2010, *J. Geophys. Res.-Atmos.*, 118, 5216-5230,  
743 <https://doi.org/10.1002/jgrd.50457>, 2013.

744 [He, K., Sun, J., and Chen, Q.: Response of climate and soil texture to net primary productivity and](https://doi.org/10.11829/j.issn.1001-0629.2019-0036)  
745 [precipitation-use efficiency in the Tibetan Plateau, \*Pratacultural Science\*, 36, 1053–1065.](https://doi.org/10.11829/j.issn.1001-0629.2019-0036)  
746 <https://doi.org/10.11829/j.issn.1001-0629.2019-0036>, 2019.

747 Hillel, D.: *Applications of Soil Physics*, Academic Press, 400 pp., 1980.

748 Hjort, J., Karjalainen, O., Aalto, J., Westermann, S., Romanovsky, V. E., Nelson, F. E., Eitzelmüller,  
749 B., and Luoto, M.: Degrading permafrost puts Arctic infrastructure at risk by mid-century, *Nat.*  
750 *Commun.*, 9, 5147, <https://doi.org/10.1038/s41467-018-07557-4>, 2018.

751 Hong, S., Yu, X., Park, S. K., Choi, Y. S., and Myoung, B.: Assessing optimal set of implemented  
752 physical parameterization schemes in a multi-physics land surface model using genetic algorithm,  
753 *Geosci. Model Dev.*, 7, 2517-2529, <https://doi.org/10.5194/gmd-7-2517-2014>, 2014.

754 Hu, G., Zhao, L., Li, R., Wu, T., Wu, X., Pang, Q., Xiao, Y., Qiao, Y., and Shi, J.: Modeling  
755 hydrothermal transfer processes in permafrost regions of Qinghai-Tibet Plateau in China, *Chin.*  
756 *Geograph. Sci.*, 25, 713-727, <https://doi.org/10.1007/s11769-015-0733-6>, 2015.

757 Hu, G., Zhao, L., Wu, X., Li, R., Wu, T., Xie, C., Pang, Q., and Zou, D.: Comparison of the thermal  
758 conductivity parameterizations for a freeze-thaw algorithm with a multi-layered soil in permafrost  
759 regions, *Catena*, 156, 244-251, <https://doi.org/10.1016/j.catena.2017.04.011>, 2017.

760 [Jiang, Y., Chen, F., Gao, Y., He, C., Barlage, M., and Huang, W.: Assessment of uncertainty sources](https://doi.org/10.1029/2020JD032674)  
761 [in snow cover simulation in the Tibetan Plateau, \*J. Geophys. Res.-Atmos.\*, 125, e2020JD032674,](https://doi.org/10.1029/2020JD032674)  
762 <https://doi.org/10.1029/2020JD032674>, 2020.

763 Jin, H., Sun, L., Wang, S., He, R., Lu, L., and Yu, S.: Dual influences of local environmental Variables  
764 on ground temperatures on the interior-eastern Qinghai-Tibet Plateau (I): vegetation and snow  
765 cover. *J. Glaciol. Geocryol.* 30, 535–545, 2008.

766 Koren, V., Schaake, J., Mitchell, K., Duan, Q. Y., Chen, F., and Baker, J. M.: A parameterization of  
767 snowpack and frozen ground intended for NCEP weather and climate models, *J. Geophys. Res.-*  
768 *Atmos.*, 104, 19569-19585, <https://doi.org/10.1029/1999JD900232>, 1999.

769 Koven, C., Riley, W., and Stern, A.: Analysis of Permafrost Thermal Dynamics and Response to  
770 Climate Change in the CMIP5 Earth System Models, *J. Clim.*, 26, 1877-1900,  
771 <https://doi.org/10.1175/JCLI-D-12-00228.1>, 2013.

772 Lawrence, D., Fisher, R., Koven, C., Oleson, K., Swenson, S., Vertenstein, M.: Technical description  
773 of version 5.0 of the Community Land Model (CLM), Boulder, Colorado, 2018.

774 Li, J., Chen, F., Zhang, G., Barlage, M., Gan, Y., Xin, Y., and Wang, C.: Impacts of Land Cover and

775 Soil Texture Uncertainty on Land Model Simulations Over the Central Tibetan Plateau, *J. Adv.*  
776 *Model. Earth Sy.*, 10, 2121-2146, <https://doi.org/10.1029/2018ms001377>, 2018.

777 [Li, K., Gao, Y., Fei, C., Xu, J., Jiang, Y., Xiao, L., Li, R., and Pan, Y.: Simulation of impact of roots](#)  
778 [on soil moisture and surface fluxes over central Qinghai – Xizang Plateau. \*Plateau Meteor.\*, 34,](#)  
779 [642-652. <https://doi.org/10.7522/j.issn.1000-0534.2015.00035>, 2015.](#)

780 Li, R., Zhao, L., Wu, T., Wang, Q. X., Ding, Y., Yao, J., Wu, X., Hu, G., Xiao, Y., Du, Y., Zhu, X.,  
781 Qin, Y., Shuhua, Y., Bai, R., Erji, D., Liu, G., Zou, D., Yongping, Q., and Shi, J.: Soil thermal  
782 conductivity and its influencing factors at the Tanggula permafrost region on the Qinghai–Tibet  
783 Plateau, *Agric. For. Meteor.*, 264, 235-246, <https://doi.org/10.1016/j.agrformet.2018.10.011>,  
784 2019.

785 [Li, X., Wu, T., Zhu, X., Jiang, Y., Hu, G., Hao, J., Ni, J., Li, R., Qiao, Y., Yang, C., Ma, W., Wen, A.,](#)  
786 [and Ying, X.: Improving the Noah-MP Model for simulating hydrothermal regime of the active](#)  
787 [layer in the permafrost regions of the Qinghai-Tibet Plateau, \*J. Geophys. Res.-Atmos.\*, 125,](#)  
788 [e2020JD032588. <https://doi.org/10.1029/2020JD032588>, 2020.](#)

789 [Luo, D., Wu, Q., Jin, H., Marchenko, S., Lyu, L., and Gao, S.: Recent changes in the active layer](#)  
790 [thickness across the northern hemisphere, \*Environ. Earth Sci.\*, 75, 555.](#)  
791 [https://doi.org/10.1007/s12665-015-5229-2, 2016.](#)

792 Luo, S., Lyu, S., Zhang, Y., Hu, Z., Ma, Y. M., Li, S. S., and Shang, L.: Soil thermal conductivity  
793 parameterization establishment and application in numerical model of central Tibetan Plateau,  
794 *Chin. J. Geophys.*, 52, 919-928, <https://doi.org/10.3969/j.issn.0001-5733.2009.04.008>, 2009.

795 Ma, N., Zhang, Y., Guo, Y., Gao, H., Zhang, H., and Wang, Y.: Environmental and biophysical  
796 controls on the evapotranspiration over the highest alpine steppe, *J. Hydrol.*, 529, 980-992,  
797 <https://doi.org/https://doi.org/10.1016/j.jhydrol.2015.09.013>, 2015.

798 Maheu, A., Anctil, F., Gaborit, É., Fortin, V., Nadeau, D. F., and Therrien, R.: A field evaluation of  
799 soil moisture modelling with the Soil, Vegetation, and Snow (SVS) land surface model using  
800 evapotranspiration observations as forcing data, *J. Hydrol.*, 558, 532-545,  
801 <https://doi.org/https://doi.org/10.1016/j.jhydrol.2018.01.065>, 2018.

802 Melton, J., Verseghy, D., Sospedra-Alfonso, R., and Gruber, S.: Improving permafrost physics in  
803 the coupled Canadian Land Surface Scheme (v.3.6.2) and Canadian Terrestrial Ecosystem Model  
804 (v.2.1) (CLASS-CTEM), *Geosci. Model Dev.*, 12, 4443-4467, [https://doi.org/10.5194/gmd-12-](https://doi.org/10.5194/gmd-12-4443-2019)  
805 [4443-2019](#), 2019.

806 Nicolsky, D. J., Romanovsky, V. E., Alexeev, V. A., and Lawrence, D. M.: Improved modeling of  
807 permafrost dynamics in a GCM land-surface scheme, *Geophys. Res. Lett.*, 34, L08501,  
808 <https://doi.org/10.1029/2007gl029525>, 2007.

809 Niu, G.-Y., and Yang, Z.-L.: Effects of vegetation canopy processes on snow surface energy and  
810 mass balances, *J. Geophys. Res.-Atmos.*, 109, D23111, <https://doi.org/10.1029/2004jd004884>,  
811 2004.

812 Niu, G.-Y., and Yang, Z.-L.: Effects of Frozen Soil on Snowmelt Runoff and Soil Water Storage at  
813 a Continental Scale, *J. Hydrometeor.*, 7, 937-952, <https://doi.org/10.1175/JHM538.1>, 2006.

814 Niu, G.-Y., Yang, Z.-L., Dickinson, R. E., and Gulden, L. E.: A simple TOPMODEL-based runoff  
815 parameterization (SIMTOP) for use in global climate models, *J. Geophys. Res.-Atmos.*, 110,  
816 D21106, <https://doi.org/10.1029/2005jd006111>, 2005.

817 Niu, G.-Y., Yang, Z.-L., Dickinson, R. E., Gulden, L. E., and Su, H.: Development of a simple  
818 groundwater model for use in climate models and evaluation with Gravity Recovery and Climate

819 Experiment data, *J. Geophys. Res.-Atmos.*, 112, D07103, <https://doi.org/10.1029/2006jd007522>,  
820 2007.

821 Niu, G.-Y., Yang, Z.-L., Mitchell, K. E., Chen, F., Ek, M. B., Barlage, M., Kumar, A., Manning, K.,  
822 Niyogi, D., and Rosero, E.: The community Noah land surface model with multiparameterization  
823 options (Noah-MP): 1. Model description and evaluation with local-scale measurements, *J.*  
824 *Geophys. Res.-Atmos.*, 116, D12109, <https://doi.org/10.1029/2010JD015139>, 2011.

825 Pan, X., Li, Y., Yu, Q., Shi, X., Yang, D., and Roth, K.: Effects of stratified active layers on high-  
826 altitude permafrost warming: a case study on the Qinghai–Tibet Plateau, *The Cryosphere*, 10,  
827 1591-1603, <https://doi.org/10.5194/tc-10-1591-2016>, 2016.

828 [Park, S., and Park, S.K.: Parameterization of the snow-covered surface albedo in the Noah-MP](https://doi.org/10.5194/gmd-9-1073-2016)  
829 [Version 1.0 by implementing vegetation effects, \*Geosci. Model Dev.\*, 9, 1073-1085,](https://doi.org/10.5194/gmd-9-1073-2016)  
830 <https://doi.org/10.5194/gmd-9-1073-2016>, 2016.

831 Pilgrim, D. H., Chapman, T. G., and Doran, D. G.: Problems of rainfall-runoff modelling in arid and  
832 semiarid regions, *Hydrolog. Sci. J.*, 33, 379-400, <https://doi.org/10.1080/02626668809491261>,  
833 1988.

834 [Qin, Y., Wu, T., Zhao, L., Wu, X., Li, R., Xie, C., Pang, Q., Hu, G., Qiao, Y., Zhao, G., Liu, G., Zhu,](https://doi.org/10.1002/2017JD026858)  
835 [X., and Hao, J.: Numerical modeling of the active layer thickness and permafrost thermal state](https://doi.org/10.1002/2017JD026858)  
836 [across Qinghai-Tibetan Plateau. \*J. Geophys. Res.-Atmos.\*, 122, 11,604-611,620,](https://doi.org/10.1002/2017JD026858)  
837 <https://doi.org/10.1002/2017JD026858>, 2017.

838 Ran, Y., Xin, L., and Cheng, G.: Climate warming over the past half century has led to thermal  
839 degradation of permafrost on the Qinghai–Tibet Plateau, *Cryosphere*, 12, 595-608,  
840 <https://doi.org/10.5194/tc-12-595-2018>, 2018.

841 Schaake, J. C., Koren, V. I., Duan, Q. Y., Mitchell, K., and Chen, F.: Simple water balance model  
842 for estimating runoff at different spatial and temporal scales, *J. Geophys. Res.-Atmos.*, 101, 7461-  
843 7475, <https://doi.org/10.1029/95jd02892>, 1996.

844 Shen, M., Piao, S., Jeong, S.-J., Zhou, L., Zeng, Z., Ciais, P., Chen, D., Huang, M., Jin, C.-S., Li, L.  
845 Z. X., Li, Y., Myneni, R. B., Yang, K., Zhang, G., Zhang, Y., and Yao, T.: Evaporative cooling  
846 over the Tibetan Plateau induced by vegetation growth, *Proc. Natl. Acad. Sci. U. S. A.*, 112, 9299-  
847 9304, <https://doi.org/10.1073/pnas.1504418112>, 2015.

848 Wang, W., Yang, K., Zhao, L., Zheng, Z., Lu, H., Mamtimin, A., Ding, B., Li, X., Zhao, L., Li, H.,  
849 Che, T., and Moore, J. C.: Characterizing Surface Albedo of Shallow Fresh Snow and Its  
850 Importance for Snow Ablation on the Interior of the Tibetan Plateau, *J. Hydrometeorol.*, 21, 815-  
851 827, <https://doi.org/10.1175/JHM-D-19-0193.1>, 2020.

852 Wei, Z., and Dong, W.: Assessment of Simulations of Snow Depth in the Qinghai-Tibetan Plateau  
853 Using CMIP5 Multi-Models, *Arct. Antarct. Alp. Res.*, 47, 611-525,  
854 <https://doi.org/10.1657/AAAR0014-050>, 2015.

855 Westermann, S., Langer, M., Boike, J., Heikenfeld, M., Peter, M., Eitzelmüller, B., and Krinner, G.:  
856 Simulating the thermal regime and thaw processes of ice-rich permafrost ground with the land-  
857 surface model CryoGrid 3, *Geosci. Model Dev.*, 9, 523-546, [https://doi.org/10.5194/gmd-9-523-](https://doi.org/10.5194/gmd-9-523-2016)  
858 2016, 2016.

859 Wetzell, P., and Chang, J.-T.: Concerning the Relationship between Evapotranspiration and Soil  
860 Moisture, *J. Clim. Appl. Meteorol.*, 26, 18-27, [https://doi.org/10.1175/1520-](https://doi.org/10.1175/1520-0450(1987)026<0018:CTRBEA>2.0.CO;2)  
861 0450(1987)026<0018:CTRBEA>2.0.CO;2, 1987.

862 Woo, M. K.: *Permafrost Hydrology*, Springer, Berlin, Heidelberg, 2012.

863 [Wu, X., and Nan, Z.: A multilayer soil texture dataset for permafrost modeling over Qinghai-Tibetan](#)  
864 [Plateau. Paper presented at 2016 IEEE International Geoscience and Remote Sensing Symposium](#)  
865 [\(IGARSS\), Beijing, China. <https://doi.org/10.1109/IGARSS.2016.7730283>, 2016.](#)  
866 Wu, X. B., Nan, Z. T., Zhao, S. P., Zhao, L., and Cheng, G. D.: Spatial modeling of permafrost  
867 distribution and properties on the Qinghai-Tibet Plateau, *Permafr. Periglac. Process.*, 29, 86-99,  
868 <https://doi.org/10.1002/ppp.1971>, 2018.  
869 [Xie, Z., Hu, Z., Ma, Y., Sun, G., Gu, L., Liu, S., Wang, Y., Zheng, H., and Ma, W.: Modeling blowing](#)  
870 [snow over the Tibetan Plateau with the community land model: Method and preliminary](#)  
871 [evaluation. \*J. Geophys. Res.-Atmos.\*, 124, 9332–9355. <https://doi.org/10.1029/2019jd030684>,](#)  
872 [2019.](#)  
873 Yang, K., Koike, T., Ye, B., and Bastidas, L.: Inverse analysis of the role of soil vertical  
874 heterogeneity in controlling surface soil state and energy partition, *J. Geophys. Res.-Atmos.*, 110,  
875 D08101, <https://doi.org/10.1029/2004jd005500>, 2005.  
876 Yang, K., Koike, T., Ishikawa, H., Kim, J., Li, X., Liu, H., Shaomin, L., Ma, Y., and Wang, J.:  
877 Turbulent Flux Transfer over Bare-Soil Surfaces: Characteristics and Parameterization, *J. Appl.*  
878 *Meteorol. Clim.*, 47, 276-290, <https://doi.org/10.1175/2007JAMC1547.1>, 2008.  
879 Yang, K., Chen, Y. Y., and Qin, J.: Some practical notes on the land surface modeling in the Tibetan  
880 Plateau, *Hydrol. Earth Syst. Sci.*, 13, 687-701, <https://doi.org/10.5194/hess-13-687-2009>, 2009.  
881 Yang, Z.-L., and Dickinson, R. E.: Description of the biosphere-atmosphere transfer scheme (BATS)  
882 for the soil moisture workshop and evaluation of its performance, *Global Planet. Change*, 13,  
883 117-134, [https://doi.org/10.1016/0921-8181\(95\)00041-0](https://doi.org/10.1016/0921-8181(95)00041-0), 1996.  
884 Yang, Z.-L., Cai, X., Zhang, G., Tavakoly, A., Jin, Q., Meyer, L., and Guan, X.: The Community  
885 Noah Land Surface Model with Multi-Parameterization Options (Noah-MP): Technical  
886 Description, 2011a.  
887 Yang, Z.-L., Niu, G.-Y., E. Mitchell, K., Chen, F., B. Ek, M., Barlage, M., Longuevergne, L.,  
888 Manning, K., Niyogi, D., Tewari, M., and Xia, Y.: The community Noah land surface model with  
889 multiparameterization options (Noah-MP): 2. Evaluation over global river basins. *J. Geophys.*  
890 *Res.-Atmos.* 116, D12110, <https://doi.org/10.1029/2010JD015140>, 2011b.  
891 [Yao, C., Lyu, S., Wang, T., Wang, J., and Ma, C.: Analysis on freezing-thawing characteristics of](#)  
892 [soil in high and low snowfall years in source region of the Yellow River, \*Plateau Meteor.\*, 38,](#)  
893 [474-483, 2019.](#)  
894 Yao, J., Zhao, L., Gu, L., Qiao, Y., and Jiao, K.: The surface energy budget in the permafrost region  
895 of the Tibetan Plateau, *Atmos. Res.*, 102, 394-407,  
896 <https://doi.org/https://doi.org/10.1016/j.atmosres.2011.09.001>, 2011.  
897 Yi, S., Zhou, Z., Ren, S., Ming, X., Yu, Q., Shengyun, C., and Baisheng, Y.: Effects of permafrost  
898 degradation on alpine grassland in a semi-arid basin on the Qinghai-Tibetan Plateau, *Environ.*  
899 *Res. Lett.*, 6, 045403, <https://doi.org/10.1088/1748-9326/6/4/045403>, 2011.  
900 Yi, S., He, Y., Guo, X., Chen, J., Wu, Q., Qin, Y., and Ding, Y.: The physical properties of coarse-  
901 fragment soils and their effects on permafrost dynamics: a case study on the central Qinghai-  
902 Tibetan Plateau, *The Cryosphere*, 12, 3067-3083, <https://doi.org/10.5194/tc-12-3067-2018>, 2018.  
903 You, Y. H., Huang, C. L., Yang, Z. L., Zhang, Y., Bai, Y. L., and Gu, J.: Assessing Noah-MP  
904 Parameterization Sensitivity and Uncertainty Interval Across Snow Climates, *J. Geophys. Res.-*  
905 *Atmos.*, 125, e2019JD030417, <https://doi.org/10.1029/2019jd030417>, 2020.  
906 [Yuan, W., Xu, W., Ma, M., Chen, S., Liu, W., and Cui, L.: Improved snow cover model in terrestrial](#)

907 [ecosystem models over the Qinghai-Tibetan Plateau, \*Agric. For. Meteor.\*, 218-219, 161-170,](#)  
908 <https://doi.org/10.1016/j.agrformet.2015.12.004>, 2016.

909 Zeng, X., Wang, Z., and Wang, A.: Surface Skin Temperature and the Interplay between Sensible  
910 and Ground Heat Fluxes over Arid Regions, *J. Hydrometeor.*, 13, 1359-1370,  
911 <https://doi.org/10.1175/JHM-D-11-0117.1>, 2012.

912 Zhang, G., Chen, F., and Gan, Y.: Assessing uncertainties in the Noah-MP ensemble simulations of  
913 a cropland site during the Tibet Joint International Cooperation program field campaign, *J.*  
914 *Geophys. Res.-Atmos.*, 121, 9576-9596, <https://doi.org/10.1002/2016jd024928>, 2016.

915 [Zhang, H., Su, Y., Jiang, H., Chao, H., and Su, W.: Influence of snow subliming process on land-](#)  
916 [atmosphere interaction at alpine wetland, \*J. Glaci. Geocry.\*, 40, 1223-1230, 2018.](#)

917 Zhang, T.: Influence of the seasonal snow cover on the ground thermal regime: An overview,  
918 *Reviews of Geophysics*, 43, RG4002, <https://doi.org/10.1029/2004RG000157>, 2005.

919 Zhao, L., Hu, G., Zou, D., Wu, X., Ma, L., Sun, Z., Yuan, L., Zhou, H., and Liu, S.: Permafrost  
920 changes and its effects on hydrological processes on Qinghai-Tibet Plateau, *Bull. Chin. Acad.*  
921 *Sci.*, 34, 1233-1246, <https://doi.org/10.16418/j.issn.1000-3045.2019.11.006>, 2019.

922 Zheng, D., Van Der Velde, R., Su, Z., Wen, J., and Wang, X.: Assessment of Noah land surface  
923 model with various runoff parameterizations over a Tibetan river, *J. Geophys. Res.-Atmos.*, 122,  
924 1488-1504, <https://doi.org/10.1002/2016jd025572>, 2017.

925 Zheng, H., Yang, Z.-L., Lin, P., Wei, J., Wu, W.-Y., Li, L., Zhao, L., and Wang, S.: On the sensitivity  
926 of the precipitation partitioning into evapotranspiration and runoff in land surface  
927 parameterizations, *Water Resour. Res.*, 55, 95-111, <https://doi.org/10.1029/2017WR022236>,  
928 2019.

929 Zheng, W., Wei, H., Wang, Z., Zeng, X., Meng, J., Ek, M., Mitchell, K., and Derber, J.: Improvement  
930 of daytime land surface skin temperature over arid regions in the NCEP GFS model and its impact  
931 on satellite data assimilation, *J. Geophys. Res.-Atmos.*, 117, D06117,  
932 <https://doi.org/10.1029/2011jd015901>, 2012.

933 Zilitinkevich, S.: Non-local turbulent transport pollution dispersion aspects of coherent structure of  
934 convective flows, *Air Pollution III, Air pollution theory and simulation* (H Power, N  
935 Moussiopoulos, C A Brebbia, eds ) *Computational Mechanics Publ* , Southampton, Boston, 1, 53-  
936 60, 1995.

937 Zou, D., Zhao, L., Sheng, Y., Chen, J., Hu, G., Wu, T., Wu, J., Xie, C., Wu, X., Pang, Q., Wang, W.,  
938 Du, E., Li, W., Liu, G., Li, J., Qin, Y., Qiao, Y., Wang, Z., Shi, J., and Cheng, G.: A new map of  
939 permafrost distribution on the Tibetan Plateau, *The Cryosphere*, 11, 2527-2542,  
940 <https://doi.org/10.5194/tc-11-2527-2017>, 2017.

941

*Supplement of*

**Assessing the simulated soil thermal regime from Noah-MP LSM  
v1.1 for near-surface permafrost modeling on the Qinghai-Tibet  
Plateau**

**Xiangfei Li et al.**

*Correspondence to:* Tonghua Wu (thuawu@lzb.ac.cn)

| Content: [Equations S1-S7](#); [Table S1](#); Figures S1-~~S4~~[S9](#)

The soil hydraulic parameters of each layer, including the porosity ( $\theta_s$ ), saturated hydraulic conductivity ( $K_s$ ), hydraulic potential ( $\psi_s$ ), the Clapp-Hornberger parameter ( $b$ ), field capacity ( $\theta_{ref}$ ), wilt point ( $\theta_w$ ), and saturated soil water diffusivity ( $D_s$ ), were determined using the pedotransfer functions proposed by Hillel (1980), Cosby et al. (1984), and Wetzel and Chang (1987):

$$\theta_s = 0.489 - 0.00126(\%sand) \quad (S1)$$

$$K_s = 7.0556 \times 10^{-6.884+0.0153(\%sand)} \quad (S2)$$

$$\psi_s = -0.01 \times 10^{1.88-0.0131(\%sand)} \quad (S3)$$

$$b = 2.91 + 0.159(\%clay) \quad (S4)$$

$$\theta_{ref} = \theta_s \left[ \frac{1}{3} + \frac{2}{3} \left( \frac{5.79 \times 10^{-9}}{K_s} \right)^{1/(2b+3)} \right] \quad (S5)$$

$$\theta_w = 0.5\theta_s \left( \frac{-200}{\psi_s} \right)^{-1/b} \quad (S6)$$

$$D_s = b \cdot K_s \cdot \left( \frac{\psi_s}{\theta_s} \right) \quad (S7)$$

where  $\%sand$  and  $\%clay$  represent the percentage (%) of sand and clay content in soil, respectively.



**Table S1** Soil discretization scheme and soil particle fraction in this study.

<u>Layer</u>	<u>Z<sub>i</sub></u>	<u>ΔZ<sub>i</sub></u>	<u>Z<sub>h,i</sub></u>	<u>Sand (%)</u>	<u>Silt (%)</u>	<u>Clay (%)</u>
<u>1</u>	<u>0.010</u>	<u>0.020</u>	<u>0.020</u>			
<u>2</u>	<u>0.040</u>	<u>0.040</u>	<u>0.060</u>	<u>85.48</u>	<u>12.59</u>	<u>1.93</u>
<u>3</u>	<u>0.090</u>	<u>0.060</u>	<u>0.120</u>			
<u>4</u>	<u>0.160</u>	<u>0.080</u>	<u>0.200</u>	<u>83.51</u>	<u>13.57</u>	<u>2.92</u>
<u>5</u>	<u>0.260</u>	<u>0.120</u>	<u>0.320</u>	<u>81.15</u>	<u>15.58</u>	<u>3.27</u>
<u>6</u>	<u>0.400</u>	<u>0.160</u>	<u>0.480</u>	<u>86.62</u>	<u>11.16</u>	<u>2.22</u>
<u>7</u>	<u>0.580</u>	<u>0.200</u>	<u>0.680</u>	<u>78.73</u>	<u>18.06</u>	<u>3.21</u>
<u>8</u>	<u>0.800</u>	<u>0.240</u>	<u>0.920</u>	<u>88.12</u>	<u>8.98</u>	<u>2.90</u>
<u>9</u>	<u>1.060</u>	<u>0.280</u>	<u>1.200</u>			
<u>10</u>	<u>1.360</u>	<u>0.320</u>	<u>1.520</u>	<u>95.00</u>	<u>3.00</u>	<u>2.00</u>
<u>11</u>	<u>1.700</u>	<u>0.360</u>	<u>1.880</u>	<u>92.50</u>	<u>4.00</u>	<u>3.50</u>
<u>12</u>	<u>2.080</u>	<u>0.400</u>	<u>2.280</u>			
<u>13</u>	<u>2.500</u>	<u>0.440</u>	<u>2.720</u>			
<u>14</u>	<u>2.990</u>	<u>0.540</u>	<u>3.260</u>	<u>90.00</u>	<u>5.00</u>	<u>5.00</u>
<u>15</u>	<u>3.580</u>	<u>0.640</u>	<u>3.900</u>			
<u>16</u>	<u>4.270</u>	<u>0.740</u>	<u>4.640</u>			
<u>17</u>	<u>5.060</u>	<u>0.840</u>	<u>5.480</u>			
<u>18</u>	<u>5.950</u>	<u>0.940</u>	<u>6.420</u>	<u>68.00</u>	<u>20.00</u>	<u>12.00</u>
<u>19</u>	<u>6.940</u>	<u>1.040</u>	<u>7.460</u>			
<u>20</u>	<u>7.980</u>	<u>1.040</u>	<u>8.500</u>			

Layer node depth (Z<sub>i</sub>), thickness (ΔZ<sub>i</sub>), and depth at layer interface (Z<sub>h,i</sub>) for default soil column.  
All in meters.

---

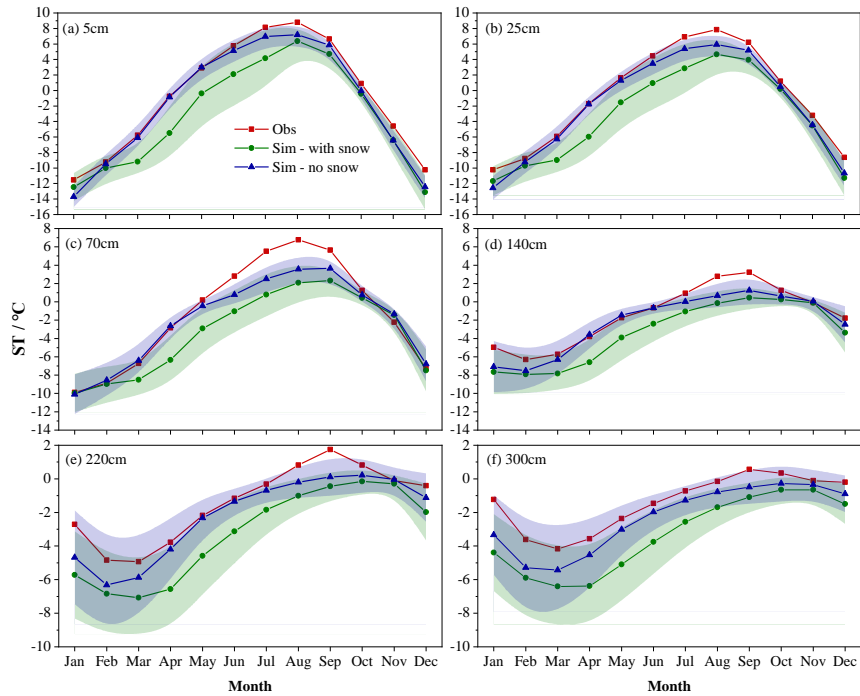


**Figure. S1.** Monthly soil temperature (ST) at (a) 5 cm, (b) 25 cm, (c) 70 cm, (d) 140 cm, (e) 220 cm, (f) 300 cm at TGL site for observation (Obs), ensemble simulation considering snow (Sim-with snow), and ensemble simulation neglecting snow (Sim-no snow). The green and blue shadow represent the standard deviation of Sim-with snow and Sim-no snow experiments, respectively.

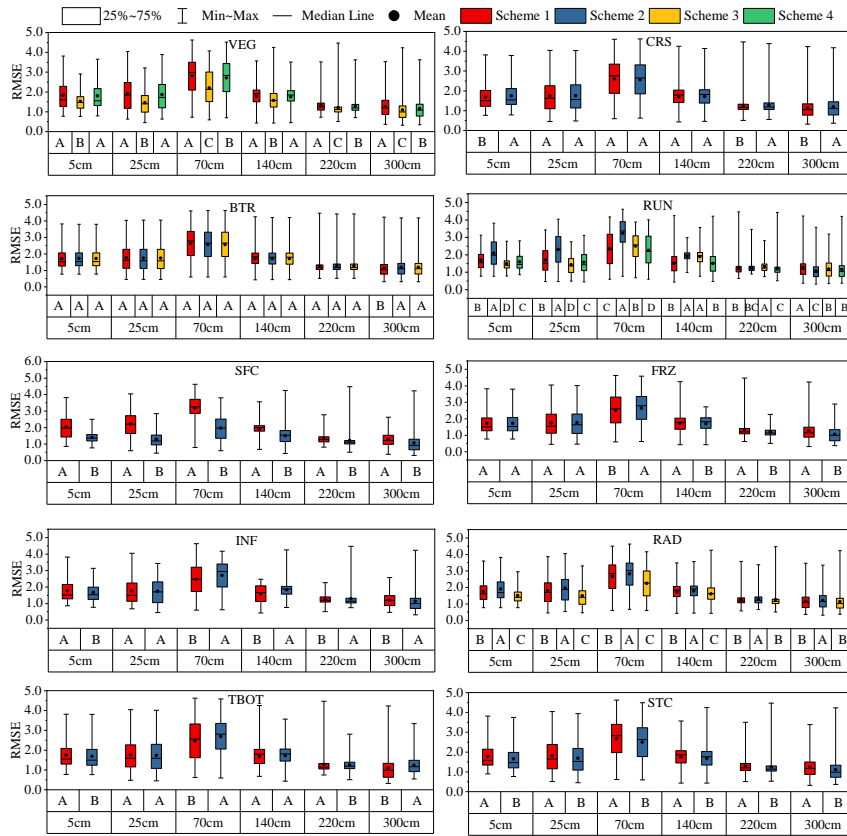


**Figure S2.** Distinction level for RMSE of ST at different layers during the warm season in the ensemble simulations. Limits of the boxes represent upper and lower quartiles, whiskers extend to the maximum and minimum RMSE. The black stations in the box are the average values. The lines in the box indicate the median value.

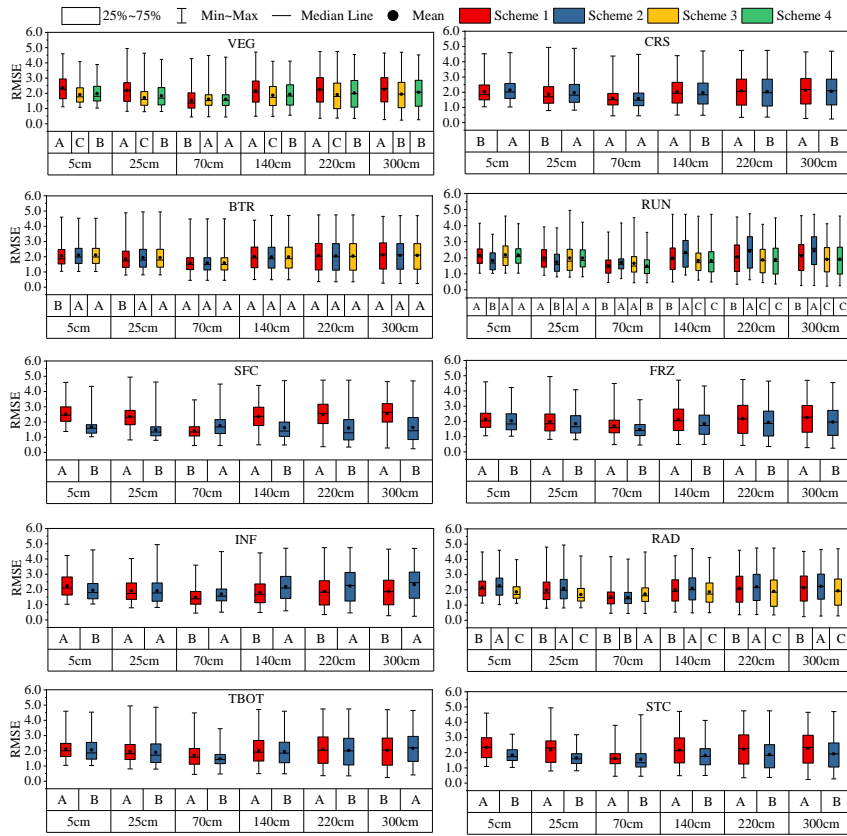


**Figure S3.** Distinction level for RMSE of ST at different layers during the cold season in the ensemble simulations. Limits of the boxes represent upper and lower quartiles, whiskers extend to the maximum and minimum RMSE. The black stations in the box are the average values. The lines in the box indicate the median value.

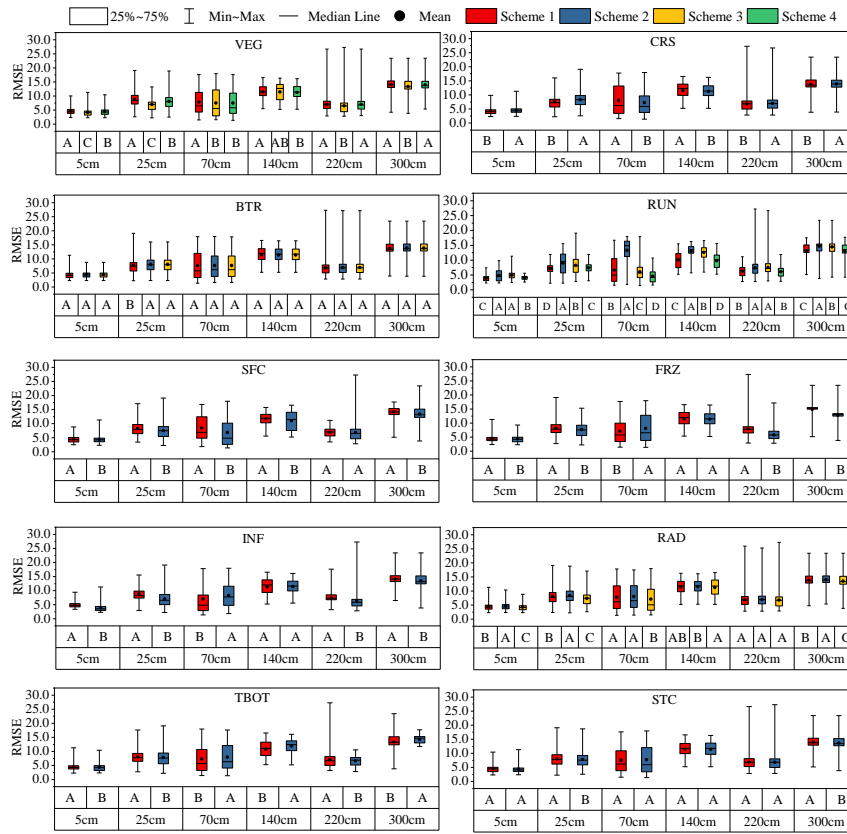


**Figure S4.** Distinction level for RMSE of SLW at different layers during the warm season in the ensemble simulations. Limits of the boxes represent upper and lower quartiles, whiskers extend to the maximum and minimum RMSE. The black stations in the box are the average values. The lines in the box indicate the median value.

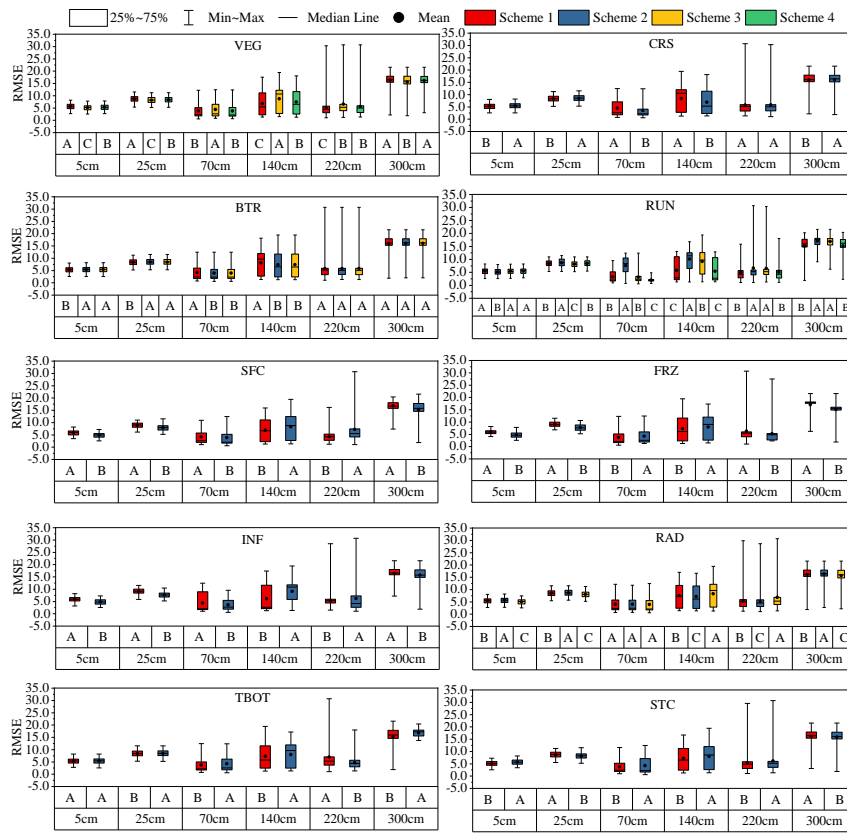
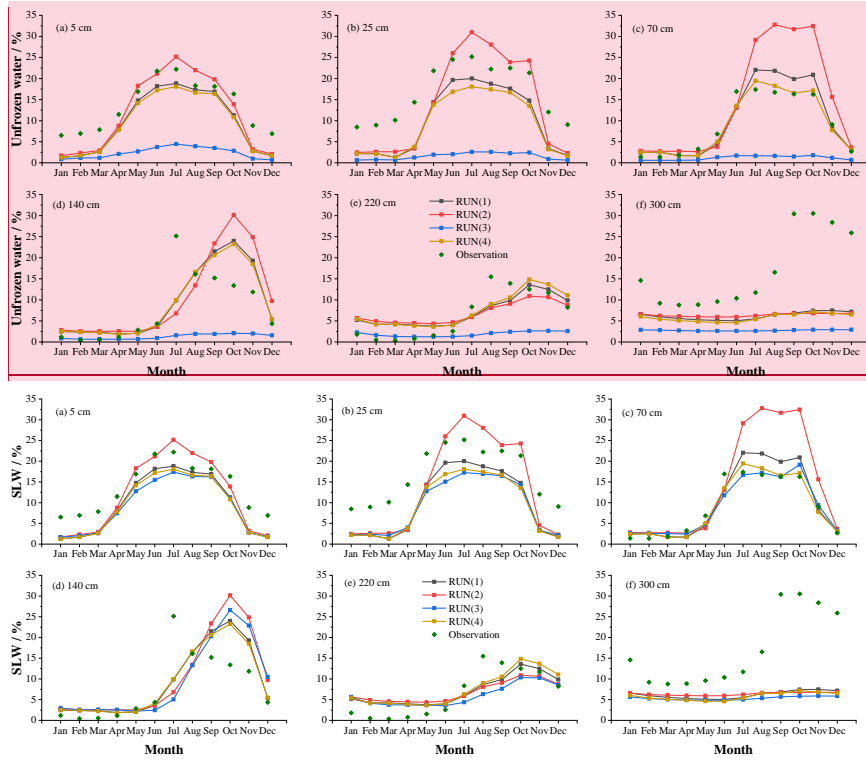
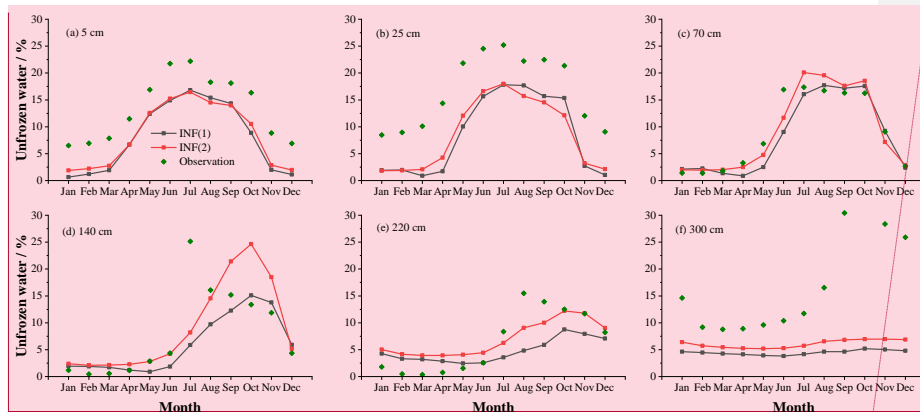


**Figure S5.** Distinction level for RMSE of SLW at different layers during the cold season in the ensemble simulations. Limits of the boxes represent upper and lower quartiles, whiskers extend to the maximum and minimum RMSE. The black stations in the box are the average values. The lines in the box indicate the median value.



批注 [LX1]: deleted

**Figure. S1-S6** Monthly unfrozen soil liquid water (SLW in %) at (a) 5 cm, (b) 25 cm, (c) 70 cm, (d) 140 cm, (e) 220 cm, (f) 300 cm for the RUN process.



批注 [LX2]: deleted

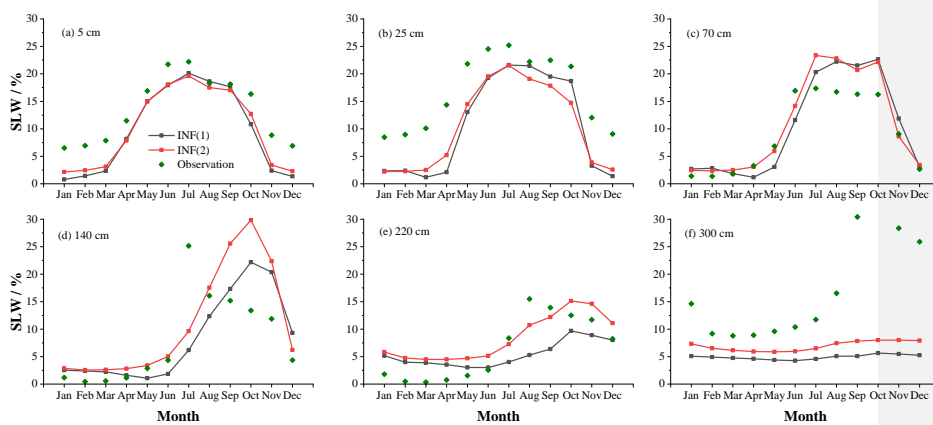
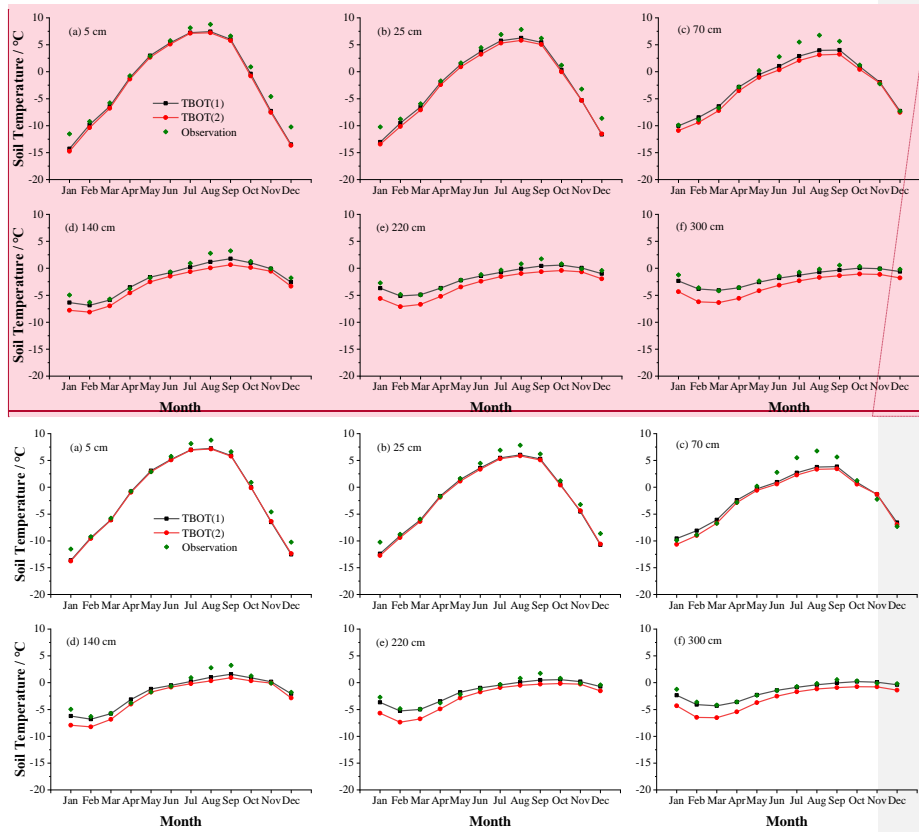


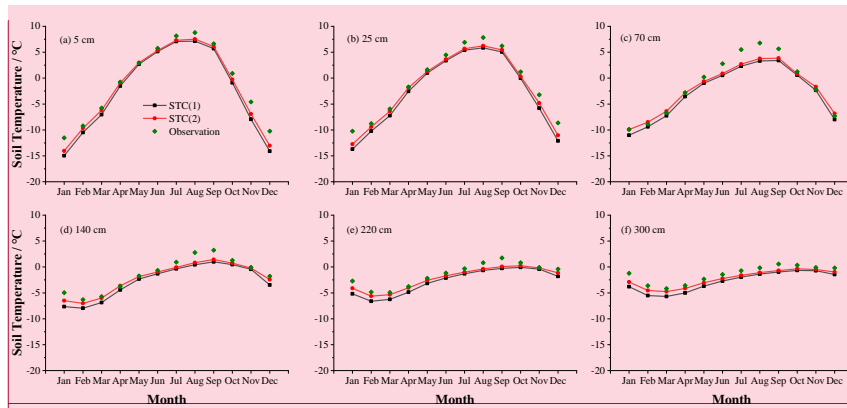
**Figure. S2-S7** Monthly unfrozen soil liquid water (SLW in %) at (a) 5 cm, (b) 25 cm, (c) 70 cm, (d) 140 cm, (e) 220 cm, (f) 300 cm for the INF process.





批注 [LX3]: deleted

**Figure. S3-S8** Monthly soil temperature at (a) 5 cm, (b) 25 cm, (c) 70 cm, (d) 140 cm, (e) 220 cm, (f) 300 cm for the TBOT process.



批注 [LX4]: deleted

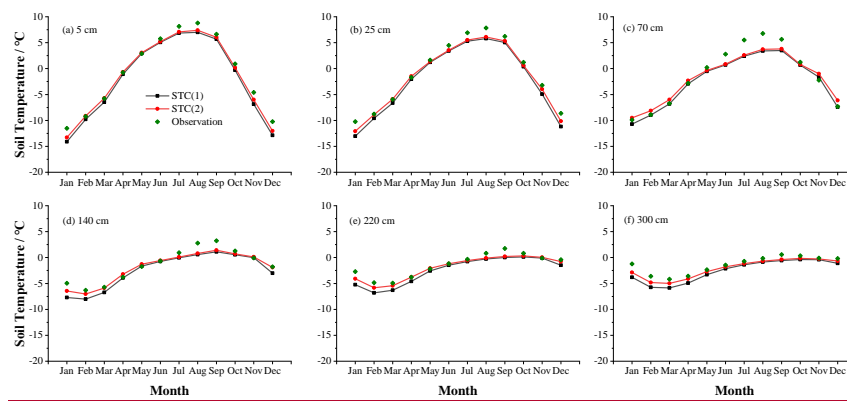


**Figure. S4-S9** Monthly soil temperature at (a) 5 cm, (b) 25 cm, (c) 70 cm, (d) 140 cm, (e) 220 cm, (f) 300 cm for the STC process.

**References:**

Hillel, D.: Applications of Soil Physics, Academic Press, 400 pp., 1980.

Cosby, B. J., Hornberger, G. M., Clapp, R. B., and Ginn, T. R.: A Statistical Exploration of the Relationships of Soil Moisture Characteristics to the Physical Properties of Soils, Water Resour. Res., 20, 682-690, <https://doi.org/10.1029/WR020i006p00682>, 1984.

Wetzel, P., and Chang, J.-T.: Concerning the Relationship between Evapotranspiration and Soil Moisture, J. Clim. Appl. Meteorol., 26, 18-27, [https://doi.org/10.1175/1520-0450\(1987\)026<0018:CTRBEA>2.0.CO;2](https://doi.org/10.1175/1520-0450(1987)026<0018:CTRBEA>2.0.CO;2), 1987.